Strategic assessment of the impacts of climate change on the Waikato region

Waikato
REGIONAL COUNCIL
Te Kaunihera ā Rohe o Waikato

Prepared by:
Yinpeng Li, Liza Storey, Wei Ye and Janet F. Bornman
University of Waikato

For:
Waikato Regional Council
Private Bag 3038
Waikato Mail Centre
HAMILTON 3240

November 2011

Document #: 2090382

Approved for release by:
Reece Hill   Date   November 2011

Strategic assessment of the impacts of climate change on the Waikato Region

Prepared by

Yinpeng Li, Liza Storey, Wei Ye and Janet F. Bornman

University of Waikato

December 2010

Executive Summary

Climate change is projected to alter long-term average climatic conditions and climatic variability in New Zealand. The best estimates are for a temperature increase of 0.2–2.0°C by 2040 and 0.7–5.1°C by 2090, with marked seasonal changes in rainfall and extreme events (Ministry for the Environment, 2008). This report provides a broad technical assessment of the physical effects of climate change in the Waikato region. Projections cover short- (2020), medium- (2050) and long-term (2100) timeframes. Ensembles (or parallel scenarios) of up to 13 Global Climate Models (GCMs) were used to generate the future scenarios. Eight climatic indices were used to represent the major climate change-induced effects, including mean temperature, mean precipitation, extreme precipitation change, peak streamflow change, Potential Evapotranspiration Deficit (PED), Temperature-Humidity Index (THI), Growing Degree Days (GDD) and sea level rise.

Baseline and future scenarios for the climate change-related indices exhibit both spatial and temporal variability across the region. The projections indicate that mean annual temperature increases by 1.20 (0.87-1.48)^{o}C by 2050 and by 2.18 (1.63-2.74)^{o}C by 2100. Summer annual mean temperature increase is the highest seasonal change: 1.29 (1.01-1.65)^{o}C by 2050 and by up to 2.45 (1.87-3.05)^{o}C by 2100.

Mean annual precipitation change is highly variable both annually and seasonally, ranging between a decrease of 4.58% and an increase of 7.19% by 2050; and between a decrease of 7.3% and an increase of 16.91% by 2100. The increase in precipitation is the highest (up to 5%) in winter, by 2050, in the southern parts of the region around the Waitomo, Otorohanga and Taupo districts. The largest decrease in precipitation is projected to occur in the Thames-Coromandel and Hauraki districts with up to 7.3% decrease in spring. The highest mean precipitation changes are projected for the Waitomo, Otorohanga, South Waikato and Taupo districts.

Extreme daily precipitation changes indicate an increase that is consistently located in north-east parts of the Waikato region – i.e., in the Hauraki and Thames-Coromandel districts and part of the Franklin district, despite projections for a decrease in annual mean precipitation by 2050 for these areas.

Peak streamflow changes are expected to increase in rivers such as the Kauaeranga and Waihou rivers which were selected for further analysis on the basis that extreme precipitation increases were projected to be highest in the areas through which these rivers flow. The Average Recurrence Intervals (ARIs) for peak streamflows are also expected to decrease (i.e. peak streamflows of specific values occur more frequently).

Projections for changes in Potential Evapotranspiration Deficit, PED, used as an indicator for drought, also highlight the spatial variability of impacts with the highest PED values (where PED>400mm) located in the Hauraki and Matamata-Piako districts by 2100. However, PED>200mm projections are more widespread across the Waikato region by 2050 and 2100, particularly in the central, northern and eastern parts. Drought-related stress on agricultural production systems and ecosystems in the Waikato region is therefore an issue that regional resource management will need to address into the future, in order to identify and assess feasible adaptation options that will ameliorate projected impacts.

The Temperature-Humidity Index, THI, indicates that mildly stress-inducing conditions (THI>72) for animals such as dairy cows are widespread across the Waikato region by 2050 and more so by 2100.

Moderately stress-inducing conditions (THI>78) are more restricted to the central parts of the Waikato region by 2050 and 2100, with two 'hotspots' evident in the Hauraki and Matamata-Piako districts and further south in the Otorohanga district, particularly by 2100.

Growing Degree Days, GDD, projections indicate that a lengthening of the growing season is expected across the entire Waikato region, although the increase is spatially variable and highest in northern districts where temperatures are warmer and lowest in the Taupo district. This projected lengthening of the growing season is likely to have beneficial effects on pasture and crop productivity, and may create opportunities for new commercial crops to be cultivated. The increase in GDD also may have an impact on native species or species of importance to biosecurity, where GDD changes are likely to induce more favourable growing conditions.

The uncertainties associated with the future projections of the eight climatic indices used in this assessment increase progressively between 2020 and 2100 scenarios, including uncertainties associated with future GHG emissions profiles, the earth's climate sensitivity to the GHG emissions, and the extent of the effects of feedback mechanisms that may influence the rate and magnitude of climate change. The uncertainty has been represented in this assessment by illustrating the spread of individual GCM projections within the various ensemble results.

Based on the findings of this Assessment, we provide recommendations for more in-depth impact assessments that will inform adaptation strategies and processes for the Waikato region. Following from this, it should be possible to identify a range of indicators and adaptation options needed to respond to the projected future effects of climate change in the Waikato region.

[Note: Detailed analyses of bio-physical impacts, risks and specific adaptation strategies for human, managed or natural systems in the region are not a part of this report. These would include impacts that affect the Regional Council's core functions and responsibilities of natural hazard management (floods, droughts and storm damage in particular), biodiversity and biosecurity management, and coastal area management, water and land management and regional planning among others. In addition, climate change has implications for regional agricultural productivity, and infrastructure that require more detailed assessments].

Table of Contents

List of Figures

List of Tables

Glossary

(Adapted from the IPCC (2007) Working Group I and Working Group II Reports)

Adaptation: An adjustment that is planned or unplanned (autonomous) within human and natural systems, in response to climatic impacts that are either experienced in the present or anticipated in the future. The adjustment is expected to reduce harmful impacts or make use of the beneficial opportunities that the climatic impacts present.

Baseline: A reference period of time against which future change is measured. The baseline may refer to climatic or non-climatic conditions and can represent an historical baseline (e.g. 1960-1990), a current baseline (including observable present-day conditions), or a future baseline (that excludes that driver factor of interest). Therefore, multiple baselines are possible, depending on how they are defined.

Climate sensitivity: The amount of global temperature rise that would occur (to a new equilibrium), when the concentration of atmospheric carbon dioxide is doubled above pre-industrial levels. In climate impact assessments, the climate sensitivity can be represented as Low, Medium or High, when generating future climate projections.

Downscaling: A method used to generate regional- to local-scale (100km-10km) climate patterns from larger scale climate models or analyses. Two main types of downscaling are in use: (1) dynamical, and (2) statistical/empirical. Statistical downscaling derives statistical relationships to link large-scale atmospheric variables to regional or local climate variables. The overall quality of downscaled climate patterns depends on the quality of the driving model.

Ensemble: A group of climate simulations from multiple climate models, used to generate future climate projections. The variations across the different simulations in the ensemble, represented by a range, are also an estimate of the uncertainty associated with the future projections. Ensembles can be made with multiple climate models (to test climate model differences) or by varying the initial conditions for a single climate model (to test internal climate variability).

General Circulation Models (GCMs) (or Global Climate Models): A numerical representation of the global climate system based on the physical, chemical and biological properties of its components, their interactions and feedback processes, and accounting for all or some of its known properties. Models of varying complexity are in use. Coupled Atmosphere-Ocean General Circulation Models (AOGCMs) provide a representation of the climate system that is near the most comprehensive end of the spectrum currently available. Climate models are applied as a research tool to study and simulate the climate, and for operational purposes, they include monthly, seasonal and inter-annual climate predictions.

Impacts: The manifested effects of climate change on natural and human systems. 'Potential' impacts refer to the total impacts that are likely to occur for a given projection of climate change, while 'residual' impacts are the impacts after taking into account the effect of adaptation measures, to reduce harm or exploit benefits of a projected climate change.

Impact assessment: A technical process that identifies and evaluates the effects of climate change on natural and human systems and that may include monetary and/or non-monetary terms. The assessment typically involves the selection of relevant climatic indices that the system under consideration is sensitive to. More detailed assessments integrate non-climatic variables (and scenarios), as well as more detailed quantitative modelling and/or qualitative information to assess changes to one or more systems.

Pattern scaling: A technique used to compare equilibrium experiments from global climate models (GCMs). The GCM patterns are then combined with simple climate model simulations to generate scenarios of regional climate change for a range of radiative forcing scenarios, for which GCM runs are not available (as it is a resource intensive process to generate a single GCM run). Pattern scaling generates accurate estimates of regional climate changes that would be simulated by a GCM under different radiative forcings (Mitchell, 2001).

Projection: A possible future evolution of a measurable variable that is typically computed with the aid of a model. Projections are different to predictions since they are subject to inherent uncertainty associated with underlying assumptions about socio-economic and technological developments at global and regional scales in the future, for instance, which are not fully known at the present time.

Scenario: A plausible, though often simplified narrative, storyline or description of how the future may develop. This narrative is based on assumptions about driving forces of change and the key relationships, and which must be internally consistent with one another. Future projections can be used to develop these scenarios in addition to other information.

Vulnerability: A measure of the degree to which a natural or human system is unable to cope with the projected adverse impacts of climate variability and change. It is a function of the magnitude and rate of climate change, as well as other factors that influence the sensitivity or exposure of the systems, as well as their capacity to adapt to the anticipated changes.

1. Introduction

Climate change will modify average climate and climate variability, thereby modifying the frequency and intensity of existing risks and hazards, as well as introducing some long-term shifts in climate regimes across New Zealand (MfE, 2008; IPCC, 2007b). Local government agencies are responsible for a range of functions that may be affected by climate change, under the Local Government Act 2002, and the Resource Management Act 1991. For regional councils, these functions may include management of regional water, and land resources, biosecurity, natural hazards management, emergency management, and regional land transport. Local authorities own community assets that may be vulnerable to climate change effects (MfE, 2008).

Based on this recognition, the Environment Waikato Regional Council requested a strategic assessment of the impacts of climate change on the Waikato region, provided in this Assessment. The results are intended to show the broad patterns of change for the region both in terms of projections of spatially-explicit climate changes and climate variability and extremes. They are also intended to provide strategic information that is relevant to planning adaptation strategies for the region. Eight climatic variables are included in this regional assessment as follows (illustrated in Figure 1):

1. Mean temperature change (Section 2.1)
2. Mean precipitation change (Section 2.1)
3. Extreme precipitation change (Section 2.2)
4. Peak streamflow change (Section 2.3)
5. Potential Evapotranspiration Deficit (PED) (Section 2.4)
6. Temperature-Humidity Index (THI) (Section 2.5)
7. Growing Degree Days (GDD) (Section 2.6)
8. Sea level rise (Section 2.7)

Global Climate Model projections (IPCC AR4)

Downscaled IPCC AR4 climate projections for New Zealand (NIWA)

Pattern-scaled regional climate patterns for the Waikato region (IGCC)

Mean temperature change

Mean precipitation change

Extreme precipitation change

Potential Evapotranspiration Deficit (PED)

Temperature-Humidity Index (THI)

Growing Degree Days (GDD)

Peak streamflow change

Sea level rise (SLR)

Figure 1 Climate change patterns for the regional climate change assessment in the Waikato.

These variables are important indices for assessing the climate–induced impacts to regional agricultural productivity, livestock stress, flood and drought-induced hazards and coastal inundation and erosion that are important to medium and long-term resource planning and management. However, to characterise the risks to specific systems (such as an agricultural production landscape, or a coastal area), it will be necessary to conduct more detailed localised assessments, for example, using risk-based modelling approaches, which are beyond the scope of the present study (key recommendations for such analyses are provided at the end of the Assessment). The data and methodologies used to produce each of the eight climate variables are described in the respective Sections 2.1-2.7.

In terms of its climate, the Waikato region is relatively sheltered by high elevation areas, which result in the predominantly cool winters with frosts and warm, dry and settled summers. Hence, the region experiences less wind than other parts of the country. Rainfall is highest in the western and eastern ranges and the Coromandel peninsula and lowest in the central Waikato basin (Kenny et al., 2001), and is influenced by the orography and prevailing wind patterns.

The Waikato region experiences less extreme climatic variations than other parts of New Zealand – particularly with respect to droughts and floods. However, over the last two decades, with the onset of more intensive dairy farming and higher stocking rates of cows, there has been a greater perception of drought risk, even in years that would otherwise be considered climatically moderate (Kenny et al., 2001). This context of dependence on agricultural production increases the climate-induced vulnerability of the region into the future.

The 12 Territorial Authority boundaries in the Waikato region are shown in Figure 2, to assist with interpreting the spatial climate scenarios produced in this Assessment.
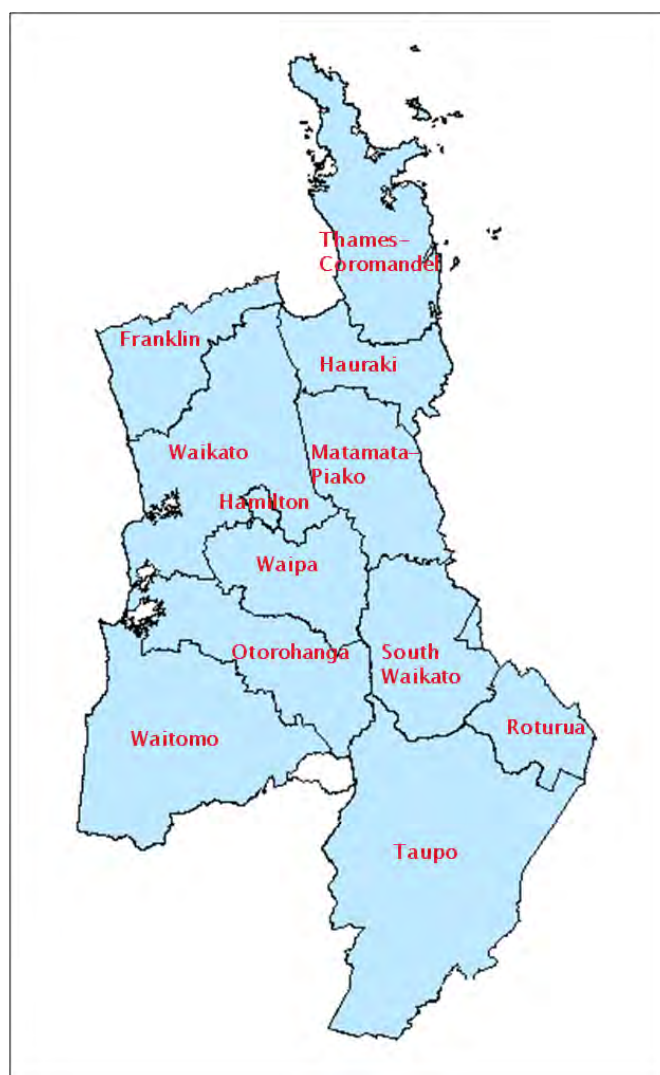
Figure 2. The Waikato region with its 12 District and City boundaries (excluding marine boundaries).

2. Baseline and future climate changes in the Waikato region

To produce the baseline and future climate projections for the Waikato region several important considerations need to be made, as they relate to assessing the impacts, risks and adaptation to climate change (Jones, 2010; and Benestad, 2002):

1. The spatial scale at which climate information is provided, to assess risks and appropriate adaptation actions;
2. There is a need for regionalised projections of climate change;
3. Local climates may exhibit gradual trends and non-linear changes in response to global warming which are usually not resolved in General Circulation Models (GCMs)[1].

The climate change scenarios produced in this Assessment are based on global General Circulation Model (GCM) outputs that are statistically downscaled for New Zealand by the National Institute for Water and Atmospheric Research (NIWA). The global GCM scenarios were downscaled to

---

[1] This is partly because of issues related to resolution, but also because the initial modelling conditions of GCMs are not set to represent current climate conditions (Jones, 2010).

0.05°latitude x 0.05° longitude by NIWA, based on the method used by Mullan et al. (2001), combined with interpolated historical monthly climate data[2].

Using the downscaled patterns, we subsequently implemented a technique called **pattern scaling** to produce climate scenarios at the scale of the Waikato region (see Appendix 1 for a full description of this method). Pattern scaling has a higher degree of confidence for temperature-related impacts, while less confidence for precipitation-related impacts of climate change can be expected. This is because attributes of climate variability and anthropogenic change are often unresolved due to large variability in precipitation patterns. As a result, systems affected by multiple variables including extreme climatic variables (for instance, agricultural cropping systems, livestock production systems and natural ecosystems), usually face higher uncertainty with respect to climate change related impacts.

Ensembles (or parallel scenarios) of up to 13 Global Climate Models (GCMs)[3] were used to generate the future scenarios, by providing the range of ensemble member values per variable. The spatial scenarios and statistics produced are presented using **ensemble statistics**, that is, the Low (10th percentile), Median (50th percentile), and High (90th percentile) values of the ensemble. (Please note: in this Assessment, all references to Low (10th), Median (50th) and High (90th) percentiles of the ensemble results will be given as 'Low', 'Median' and 'High' respectively). The GCMs selected for the ensembles are those that perform the best in terms of modelled climate for New Zealand (Mullan and Dean, 2009). Details of the GCMs used for producing the future scenarios of specific variables are provided in Appendices 3-6.

The following steps were undertaken to produce the results contained in this Assessment (and further details of the steps are provided in Appendix 1):
1. Temperature and precipitation patterns were normalised, using the global mean temperature change of the corresponding period and GCM; and
2. Spatial and statistical analyses were undertaken based on the ensemble results, for: (a) the Baseline period (1972-2008, from observed climate data from NIWA), and (b) three future time periods: 2020, 2050 and 2100, for the different variables.

To generate the future climate patterns, three greenhouse gas emissions scenarios from the Special Report on Emission Scenarios (SRES) (IPCC, 2000), were used: (1) B1 (Low GHG emissions scenario), (2) A1B (Business-As-Usual, BAU, GHG emissions scenario), and (3) A1FI (Fossil Fuel Intensive, High GHG emissions scenario). Further descriptions of the SRES scenarios are provided in Appendix 2, indicating the representative conditions that produce these alternative emissions pathways.

Figure 3 shows the global mean temperature change projected for each of the three SRES scenarios selected, between 1990 and 2100. Global GHG emissions pathways follow a similar trajectory up to ca 2020 then begin to diverge after 2025 under B1 and after 2035 for A1B and A1FI. Global mean temperature change projected under B1 and A1B converge at 0.56**°**C (or 0.60**°**C under A1FI) by 2020 and by 2100, global mean temperature ranges between 1.88**°**C (B1) and 4.41**°**C (A1FI) (Table 1). This illustrates the dependency on the future emissions trajectories, at the global scale, on the resultant global mean temperature change.

---

[2] From the NIWA CliFLO database (http://cliflo.niwa.co.nz/)
[3] Each GCM result is referred to as an ensemble 'member'.
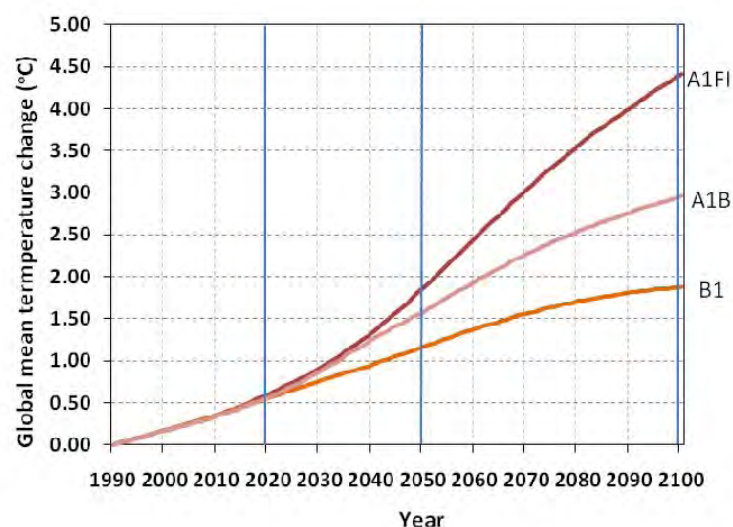
Figure 3. The global mean temperature change of the three selected SRES scenarios. The graph shows that up to 2020, global mean temperature is projected to increase by 0.5°C, irrespective of the SRES scenario and subsequently the future temperature change projections diverge by 2050 and even more by 2100, depending on the SRES scenario. (SRES, Special Report on Emissions Scenarios, Intergovernmental Panel on Climate Change (IPCC, 2001)).

Table 1. Global annual mean temperature change (°C) in the selected scenarios and times slices.

GMT change	2020	2050	2100
B1	0.56	1.17	1.88
A1B	0.56	1.58	2.96
A1FI	0.60	1.87	4.41

The following Sections 3.1-3.7 of the report provide the baseline and future scenarios of the 8 climatic variables selected for this regional assessment.

2.1 Mean temperature and precipitation changes

2.1.1 Introduction

Mean temperature and precipitation changes are two fundamental and widely measured climate variables, from which various other climate-related variables are derived. Temperature changes are one of the most easily measured changes in climate, while precipitation measurements are more difficult, often due to the influence of local wind patterns of measurement gauges (IPCC, 2007a). Changes in mean temperature and precipitation can have direct and indirect impacts on natural and human systems, depending on the direction and magnitude of the change, and the sensitivity of those systems to the resultant climate changes (Thuiller et al., 2005; Patz et al., 2005). Seasonal variations in mean temperature and precipitation influence evapotranspiration rates and soil water content, plant photosynthetic activity, metabolic processes of plants and animals, (Dai et al., 2004; Root et al., 2003; and Woodward, 1987), and stream-water flows (Brito-Castillo et al., 2003) to name a few.

2.1.2   Methodology and data

Mean temperature and precipitation were derived using the pattern scaling method described in Appendix 1. The climate data used to generate the baseline climate were provided by NIWA (as gridded climate data) for the period 1972-2008. The 12 GCMs selected for generating the future climate change scenarios are listed in Appendix 3.

2.1.3   Results

The **normalised annual mean temperature change patterns,** per degree global warming for the Waikato region indicates that annual mean temperature change is 0.70-0.76^{o}C (Median) per degree global warming. Therefore, annual mean temperature changes at a lower rate in the Waikato region compared to the global scale. Even at the High (90th percentile) of mean temperature change, the temperature increase is still lower than global mean temperature increase.
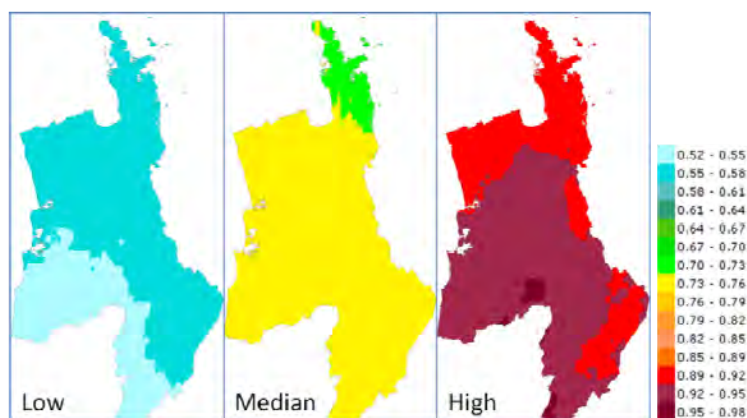
Figure 4. Normalised annual mean temperature change patterns (^{o}C per degree global mean temperature increase): using the 12-GCM ensemble for Low (10th), Median (50th), and High (90th) percentiles.

2.1.3.1 Baseline and future mean annual and seasonal temperature

Using the baseline climate data and normalised change patterns, it is possible to produce the future projections for any SRES emissions scenario and time period. To produce the patterns in Figure 5, only the Median ensemble values of the 2050 scenarios were used.

Annual mean temperature is projected to increase by 1.20 (0.87-1.48)^{o}C by 2050 (A1B) and by 2.18 (1.63-2.74)^{o}C by 2100 (A1B) (Table 2). Under a low emission scenario, B1, the temperature increases only by 1.43 (1.02, 1.74) ^{o}C, while for the high emission scenario, A1FI, the temperature will increase significantly by up to 3.37 (2.49-4.0)^{o}C for Waikato region.

The summer (DJF) mean temperature increases faster than for the other seasons with median change of 1.29 (1.01-1.65)^{o}C by 2050 (A1B) and by up to 2.45 (1.87-3.05)^{o}C by 2100 (A1B). Winter (JJA) mean temperature increases by 1.21 (0.87-1.46)^{o}C by 2050 (A1B) and up to 2.26 (1.67-2.65)^{o}C by 2100 (A1B). Spring (SON) has the slowest temperature increase among the seasons.

Table 2. Mean seasonal and annual temperature changes: B1, A1B and A1FI using Low, Medium, and High percentiles of the ensemble, for 2020, 2050 and 2100. DJF, December-January-February; MAM, March-April-May; JJA, June-July-August; SON, September-October-November; ANN, Annual mean.

		B1			A1B			A1FI		
		Low	Med	High	Low	Med	High	Low	Med	High
	2020	0.36	0.47	0.59	0.36	0.47	0.59	0.38	0.49	0.62
DJF	2050	0.75	0.97	1.23	1.01	**1.29**	1.65	1.21	1.53	1.96
	2100	1.23	**1.55**	1.96	1.87	**2.45**	3.05	2.78	**3.68**	4.63
	2020	0.33	0.43	0.50	0.33	0.43	0.50	0.36	0.44	0.53
MAM	2050	0.68	0.88	1.01	0.90	1.22	1.42	1.08	1.42	1.69
	2100	1.09	1.43	1.70	1.74	2.19	2.61	2.52	3.37	3.95
	2020	0.31	0.43	0.50	0.31	0.43	0.50	0.33	0.45	0.54
JJA	2050	0.63	0.88	1.06	0.87	**1.21**	1.46	1.01	1.43	1.72
	2100	1.02	**1.44**	1.72	1.67	**2.26**	2.65	2.48	**3.39**	3.98
	2020	0.25	0.37	0.49	0.25	0.37	0.49	0.26	0.39	0.50
SON	2050	0.51	0.76	1.00	0.69	1.02	1.32	0.81	1.25	1.56
	2100	0.82	1.25	1.57	1.29	1.97	2.50	1.94	2.93	3.73
	2020	0.31	0.42	0.51	0.31	0.42	0.51	0.33	0.44	0.55
ANN	2050	0.64	0.87	1.07	0.87	**1.20**	1.48	1.02	1.42	1.74
	2100	1.02	**1.43**	1.74	1.63	**2.18**	2.74	2.49	**3.37**	4.00
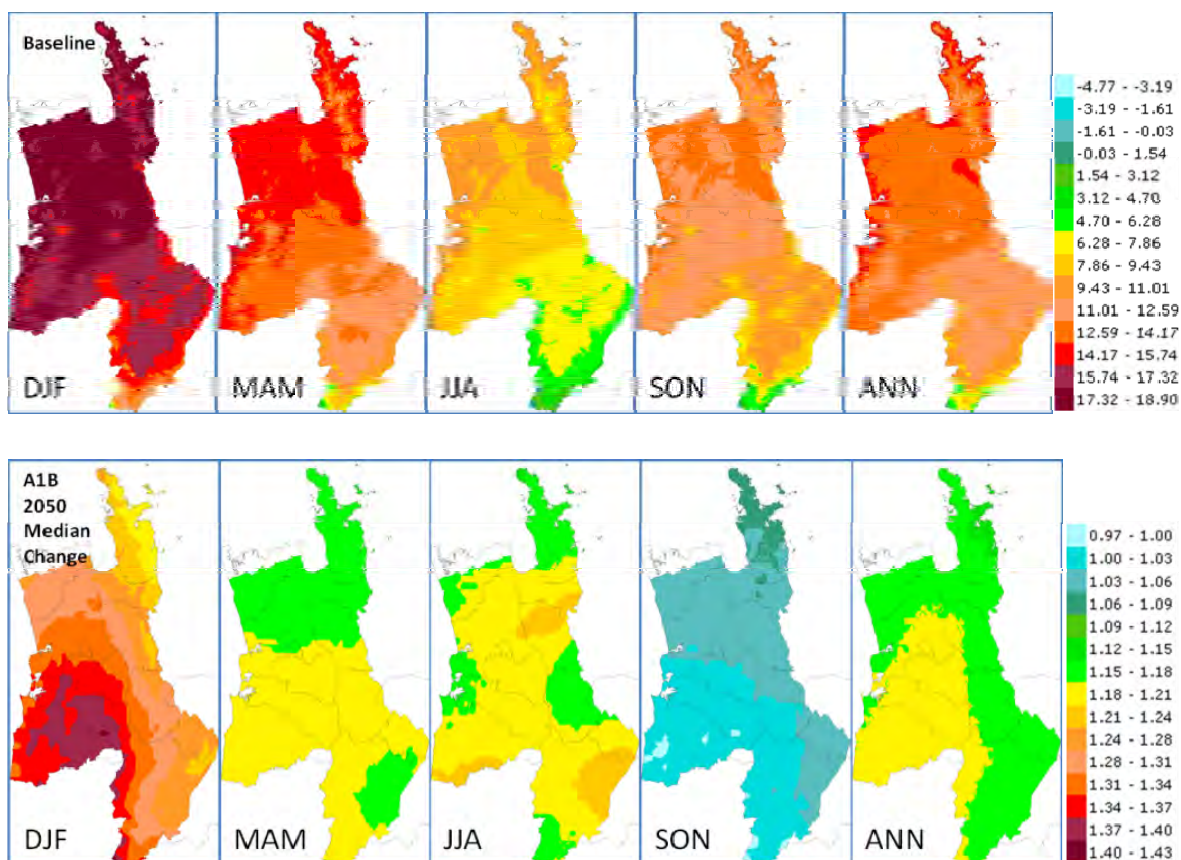
Figure 5. Mean seasonal and annual temperature change by 2050 (A1B-Median): Baseline (top panel) and 2050 (A1B, Median) (bottom panel). DJF, -December-January-February; MAM, March-April-May; JJA, June-July-August; SON, September-October-November; ANN, Annual mean.

Summer, December-January-February (DJF) mean temperature increase is projected to be the highest, with maximum temperature increases situated in parts of the Waitomo, Otorohanga and Waipa districts in the south of the region. Spring, September-October-November (SON) mean temperature increases the least of the four seasons by the year 2050 (Figures 5 and 6).

Seasonal and annual mean temperature changes are shown in Figure 6, by their Median (heavy black lines in blue boxes), Low, and High percentiles (indicated by the bottom and top of the blue boxes, respectively). The size of the boxes indicates the spread of the modelled values by each of the 12 GCMs in the ensemble and is also a measure of the uncertainty associated with the projections at each time period, such that larger boxes indicate higher associated uncertainty among GCMs, typical of scenarios for 2100.
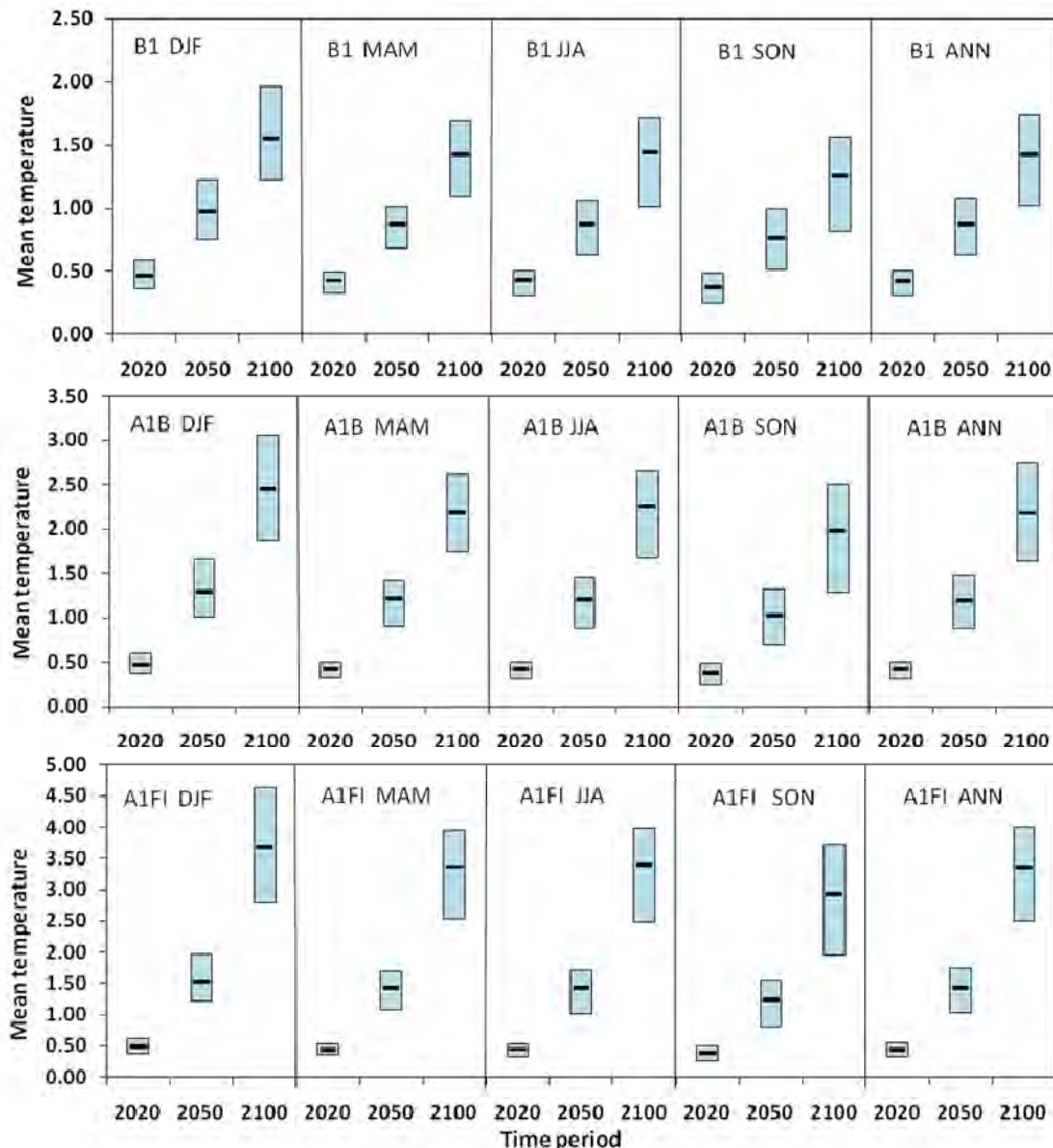
Figure 6. Statistics on the mean seasonal and annual temperature changes: B1 (top), A1B (middle) and A1FI (bottom panel), for 2020, 2050, and 2100. DJF, December-January-February; MAM, March-April-May; JJA, June-July-August; SON, September-October-November; ANN, Annual mean.

2.1.3.2 Baseline and future precipitation projections

The **normalised annual mean precipitation change patterns** in the Waikato region, show variability that is characteristic of precipitation projections, which are largely dependent on whether the projected westerly winds show an increase or a decrease across New Zealand (MfE, 2008).

Figure 7 indicates that annual mean precipitation change is projected to be between a 1.7% decrease to 2.1% increase in precipitation (Median), per degree global warming. To put the variability of the precipitation projections in context, the Low 10th percentile shows a decrease of 1.7-5.4% and the High 90th percentile shows an increase of 2.1-5.8%. Therefore, mean annual precipitation changes are projected to be relatively low, using the 12-GCM ensemble.
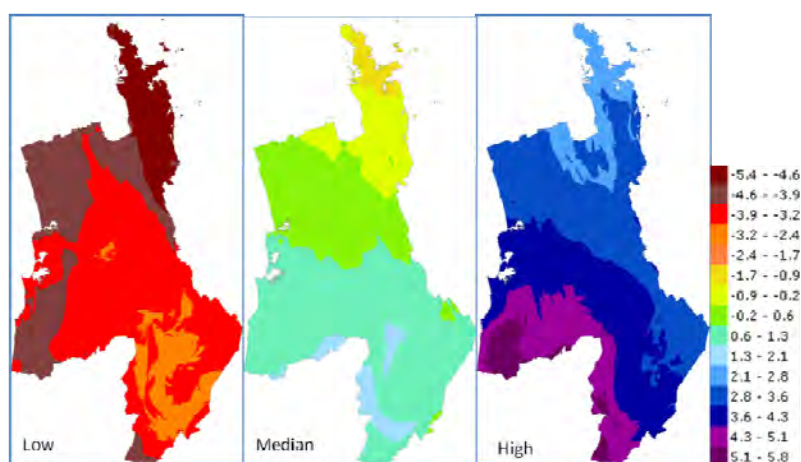
Figure 7. The normalised mean annual precipitation change (percent per degree global warming). Patterns show the Low, Median, and High of a 12-GCM ensemble.

The **annual mean monthly precipitation changes** project both increases and decreases that are spatially variable. Annual mean precipitation shows a minimal increase of 0.26 (-6.15, 6.08)% (A1B) by 2050 and 0.48 (-11.57, 11.35)% increase by 2100 (A1B), though the range of values indicate both significant increases and decreases (Table 3). The low Median precipitation values therefore should be interpreted in the context of the inherent variability that is evident in the precipitation projections.

Seasonal mean precipitation changes include projections for winter (JJA) mean precipitation increasing the most with up to 1.78 (-2.77, 7.34)% increase by 2050 (A1B) and 3.34 (-5.19, 13.75)% increase by 2100 (A1B). Summer (DJF) mean precipitation is projected to increase by 0.71 (-6.74, 7.09)% by 2050 (A1B) and by 1.33 (-12.58, 13.18)% by 2100 (A1B).

Table 3. Seasonal and annual mean precipitation changes (in percent): 2020, 2050 and 2100 scenarios using B1, A1B and A1FI, Low, Medium, and High percentiles of the 12-GCM ensemble. DJF, December-January-

		B1			A1B			A1FI		
		Low	Med	High	Low	Med	High	Low	Med	High
	2020	-2.38	0.25	2.51	-2.38	0.25	2.51	-2.55	0.27	2.69
DJF	2050	-4.96	0.53	5.27	**-6.74**	**0.71**	**7.09**	-7.96	0.84	8.41
	2100	-8.01	0.84	8.45	**-12.58**	**1.33**	**13.18**	-18.77	1.98	19.69
	2020	-2.29	0.06	1.89	-2.29	0.06	1.89	-2.44	0.06	2.03
MAM	2050	-4.77	0.12	3.95	-6.42	0.16	5.35	-7.59	0.19	6.32
	2100	-7.63	0.19	6.36	-12.06	0.30	9.96	-17.96	0.45	14.88
	2020	-0.98	0.63	2.60	-0.98	0.63	2.60	-1.05	0.68	2.79
JJA	2050	-2.04	1.32	5.43	**-2.77**	**1.78**	**7.34**	-3.28	2.11	8.68
	2100	-3.30	2.12	8.73	**-5.19**	**3.34**	**13.75**	-7.71	4.97	20.47
	2020	-3.40	-0.71	1.55	-3.40	-0.71	1.55	-3.65	-0.76	1.65
SON	2050	-7.13	-1.48	3.22	-9.57	-2.01	4.35	-11.37	-2.38	5.15
	2100	-11.42	-2.39	5.17	-18.00	-3.76	8.12	-26.80	-5.59	12.15
	2020	-2.21	**0.09**	2.15	-2.21	**0.09**	2.15	-2.34	**0.10**	2.30
ANN	2050	-4.58	**0.19**	4.49	**-6.15**	**0.26**	**6.08**	-7.26	**0.30**	7.19
	2100	-7.30	**0.31**	7.23	**-11.57**	**0.48**	**11.35**	-17.33	**0.72**	16.91

Figure 8 shows that northern districts of the region are projected to face decreases in annual mean precipitation, while southern districts are projected to experience increases. In terms of seasonal patterns, summer (DJF) mean precipitation increase is highest in the south-eastern parts of the Waikato region located mainly in the Taupo, Rotorua and Thames-Coromandel districts. The largest decrease in seasonal mean temperature is projected in spring (SON) in the Thames-Coromandel and Hauraki districts and to a lesser extent through the Matamata-Piako, Franklin, Waikato and central districts.
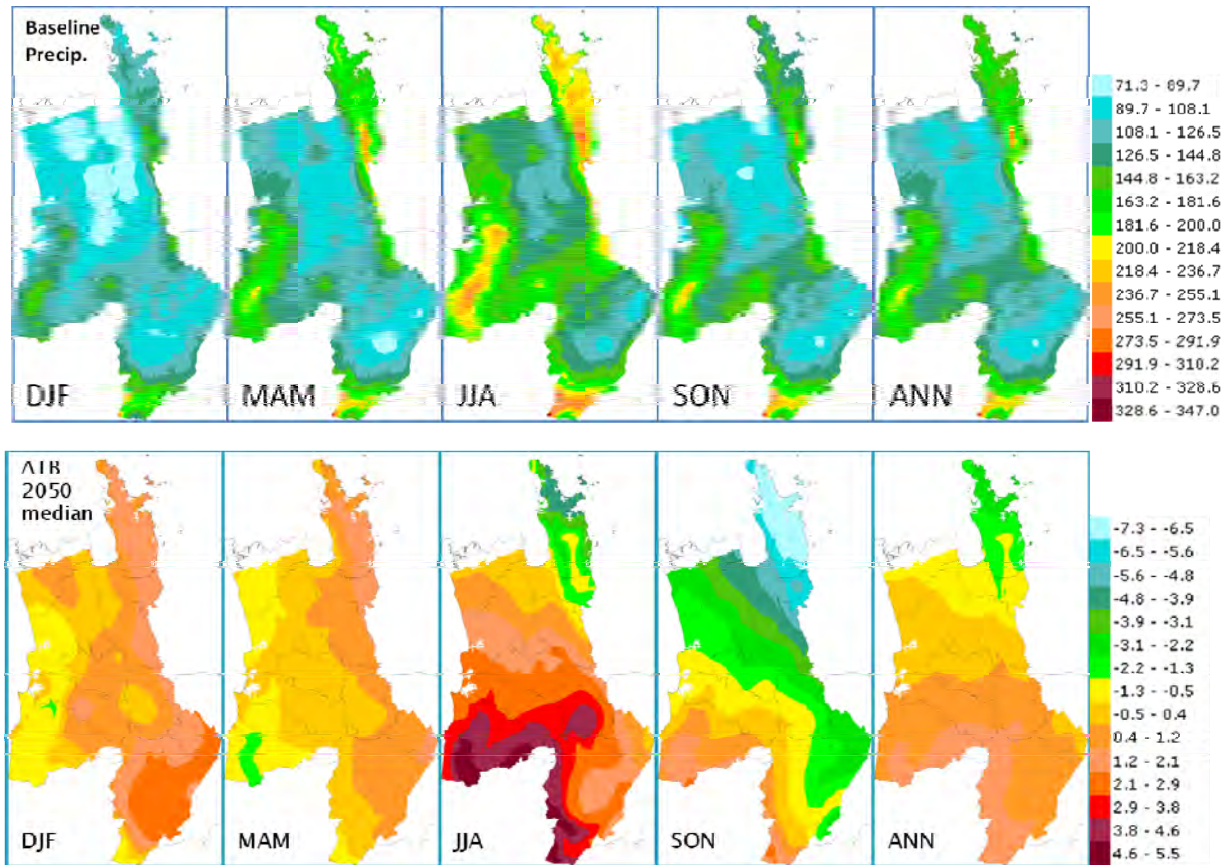
Figure 8. Mean seasonal and annual precipitation changes: Baseline (top panel) and 2050 scenario (A1B-Median) (bottom panel). DJF, December-January-February; MAM, March-April-May; JJA, June-July-August; SON, September-October-November; ANN, Annual mean.

Mean monthly precipitation change in the Waikato region is relatively small for 2020 and 2050 and by 2100 it is characterised by a large spread among GCMs (indicated by the larger blue boxes in Figure 9). This is despite a negligible change in the median value among 2020, 2050 and 2100 results. These variations are the result of different GCM model projections of mean precipitation change for each time period and season. They also indicate that uncertainty associated with the future projections is the highest for 2100 scenarios and in highest for the summer and spring seasons of the 2100 (A1FI) scenarios.
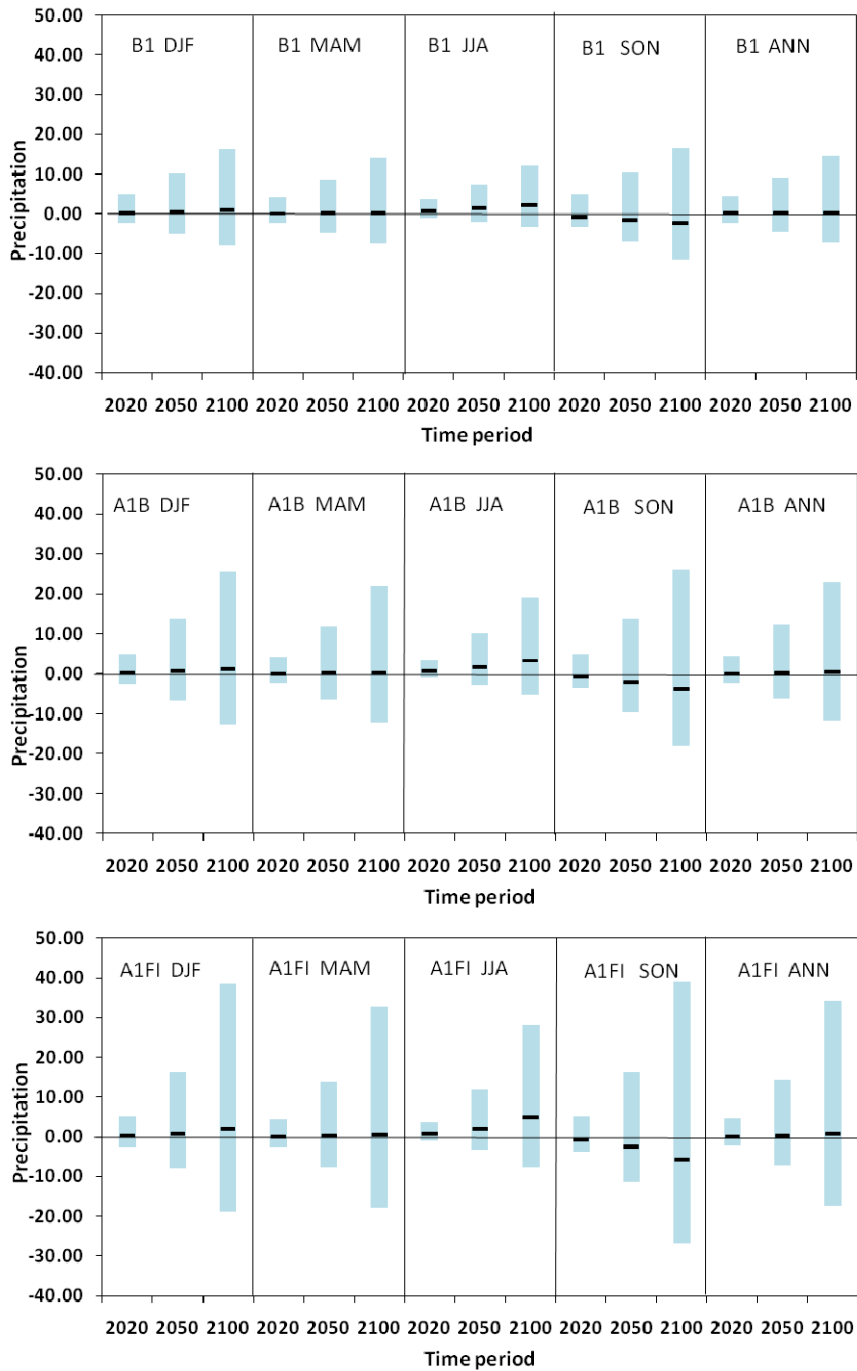
Figure 9. Statistics of mean monthly precipitation change: 12-GCM ensemble range illustrated by the blue boxes, B1 (top panel), A1B (middle) and A1FI (bottom panel) scenarios. The black line represents the Median of the ensemble results for each time horizon, 2020, 2050 and 2100.

2.1.4   Discussion and Conclusions

The projected changes in mean annual temperature relative to the baseline period of 1972-2008, are consistent with earlier values modelled in the national assessment for the Waikato region (MfE, 2008). By 2050, annual mean temperature is projected to increase by 1.20 (0.64-1.74)°C and by 2.18 (1.02-4.00)°C by 2100 (Table 2). Mean annual precipitation changes both in magnitude and direction, although changes are relatively small and exhibit more spatial variability than mean annual

temperature over the region. On the other hand, it should be noted that precipitation extremes, are projected to change more markedly, and will be addressed in Section 2.2 of this Assessment. The magnitude of the change for both mean annual temperature and precipitation is dependent on the emissions scenario for the future (B1 projecting lowest change values and A1FI projecting highest change values).

When results are aggregated across B1, A1B and A1FI for the 2050 scenarios (Table 2), mean seasonal and annual temperature changes are: 1.29 (0.75, 1.96)^{o}C in Summer, 1.22 (0.68, 1.69)^{o}C in Autumn, 1.22 (0.63, 1.72)^{o}C in Winter, 1.02 (0.51, 1.56)^{o}C in Spring, and 1.20 (0.64, 1.74)^{o}C for the Annual mean by 2050. These results for 2050 and 2100 are comparable with those of the Ministry for the Environment (MfE, 2008, pgs. 16 and 17); however, the time scales used are not exactly the same and may explain why our results report slightly higher change values. MfE (2008) used 2040 (2030–2049) and 2090(2080–2099), while we have used 2050 and 2100, respectively.

The projected changes in mean seasonal and annual precipitation change, relative to the baseline period (1972-2008), when aggregated across B1, A1B and A1FI for the 2050 scenarios (Table 3) are: 0.71 (-4.96, 8.41)% in Summer, 0.16 (-4.77, 6.32)% in Autumn, 1.78 (-2.04, 8.68)% in Winter, -2.01 (-7.13, 5.15)% in Spring, and 0.26 (-4.58, 7.19)% for the Annual mean by 2050. By comparison with MfE (2008, pg. 24), this report shows lower change values for mean seasonal precipitation projections, and this may be due to the selection of different ensemble percentile thresholds between the two studies.

There are variations in the direction of change in projected mean seasonal and annual precipitation change (projections for both increases and decreases). Therefore, it is recommended that Council needs to assess areas where decreases are projected, and how these are spatially connected to areas where increases are projected, particularly through increased river and stream flow volumes in headwaters (MfE, 2008).

2.2   Extreme precipitation change

2.2.1   Introduction

Precipitation extremes refer to extreme high or low precipitation events over time and are linked to flood and drought-related events (Sansom and Renwick, 2007). As a result, these extremes have attracted considerable research focus due to the potential hazards these present to human and natural systems. Extreme precipitation events are projected to increase with climate change, even in areas where the total precipitation is projected to decrease (Meehl et al., 2007), since global warming will noticeably enhance the hydrological cycle at both global and local scales. In most mid to high latitude and tropical areas, precipitation extremes are expected to increase more than mean precipitation, as is also projected for New Zealand (MfE, 2010; Meehl et al., 2007).

2.2.2   Methodology and data

In order to assess adequately the climate change impact on extreme precipitation events, the characteristics of GCM-simulated precipitation and its relationship to global warming need to be evaluated (Perkins et al. 2007; Alexandra and Arblaster 2008). Additionally, the evaluation of observed and modelled trends has shown that the confidence in GCM projected extremes of precipitation is much less than that of temperature (e.g. Kharin et al. 2007, Kiktev et al. 2007).

In general, the magnitude of changes in precipitation extremes simulated by GCMs is found to have a linear relationship with the strength of GHG emissions or is in proportion to the global warming trend (Alexander and Arblaster 2009, Tebaldi et al. 2006), which corresponds with the linear

response theory of pattern scaling. For the extreme precipitation change analysis undertaken in this assessment, Appendix 3 provides further details of the methodology implemented and lists the 12 GCMs used to produce the ensemble projections.

2.2.3 Results

The **normalised changes to extreme daily precipitation** (percentage changes) relative to the baseline period are shown in Table 4, for Average Recurrence Intervals (ARIs) ranging between 5-300 years. The extreme daily precipitation changes between 8.47% (for a 5-year ARI) and 11.69% (for a 300-year ARI) (Median), and a 100-year ARI is projected to change by 10.53%. (Note: the percent change in extreme daily precipitation under the Low and High percentiles of the 12-GCM ensemble also should be considered in assessing the changes for each ARI).

Table 4. Normalised extreme daily precipitation changes (percentage change). The average Recurrence Intervals (ARI) tested range from 5 to 300 years, for Low, Median and High percentiles of the 12-GCM ensemble.

ARI (year)		5	10	15	20	30	40	50	100	150	200	300
Low	%	5.46	4.93	4.62	4.81	6.09	7.02	7.54	7.72	7.73	7.75	7.76
Median	%	8.47	8.58	8.77	8.99	9.34	9.6	9.8	10.53	11.05	11.41	11.69
High	%	12.33	12.5	12.75	13.16	13.86	14.39	14.82	16.24	17.14	17.81	18.79

2.2.3.1 Baseline and future projections of extreme precipitation changes

The **extreme precipitation intensity** for an event with a 20-year ARI changes from a maximum of ca 302.0mm/day (baseline) up to a maximum of ca 410.0mm/day by 2100 (A1B); for a 50-year ARI changes from ca 360.6mm/day (baseline) to 493.8mm/day by 2100 (A1B); and a 100-year event changes from a maximum of ca 410.8mm/day (baseline) up to a maximum of 566.2mm/day by 2100 (A1B) (Figure 10).

The most extreme daily precipitation values are consistently located in the north-eastern parts of the Waikato region – in the Hauraki district, and north into the Thames-Coromandel district, and parts of the Franklin district, particularly by 2050 and 2100. Thames-Coromandel, in particular, shows consistently higher values spatially distributed across the whole district– a pattern that is not evident anywhere else in the Waikato region, and could be associated with the relatively small and steep catchments characteristics of the district.

Future projections under all scenarios tested indicate that extreme daily precipitation change values will increase. This is despite mean annual and seasonal precipitation scenarios showing both positive and negative changes that are spatially variable (refer to Figures 8 and 9 and Table 3).

The range of values projected by the different GCMs varies more widely by 2100 (illustrated by the size of the green bars in Figure 11) which is a measure of the spread and uncertainty associated with the projections by the 12-GCM model simulations by this time period.
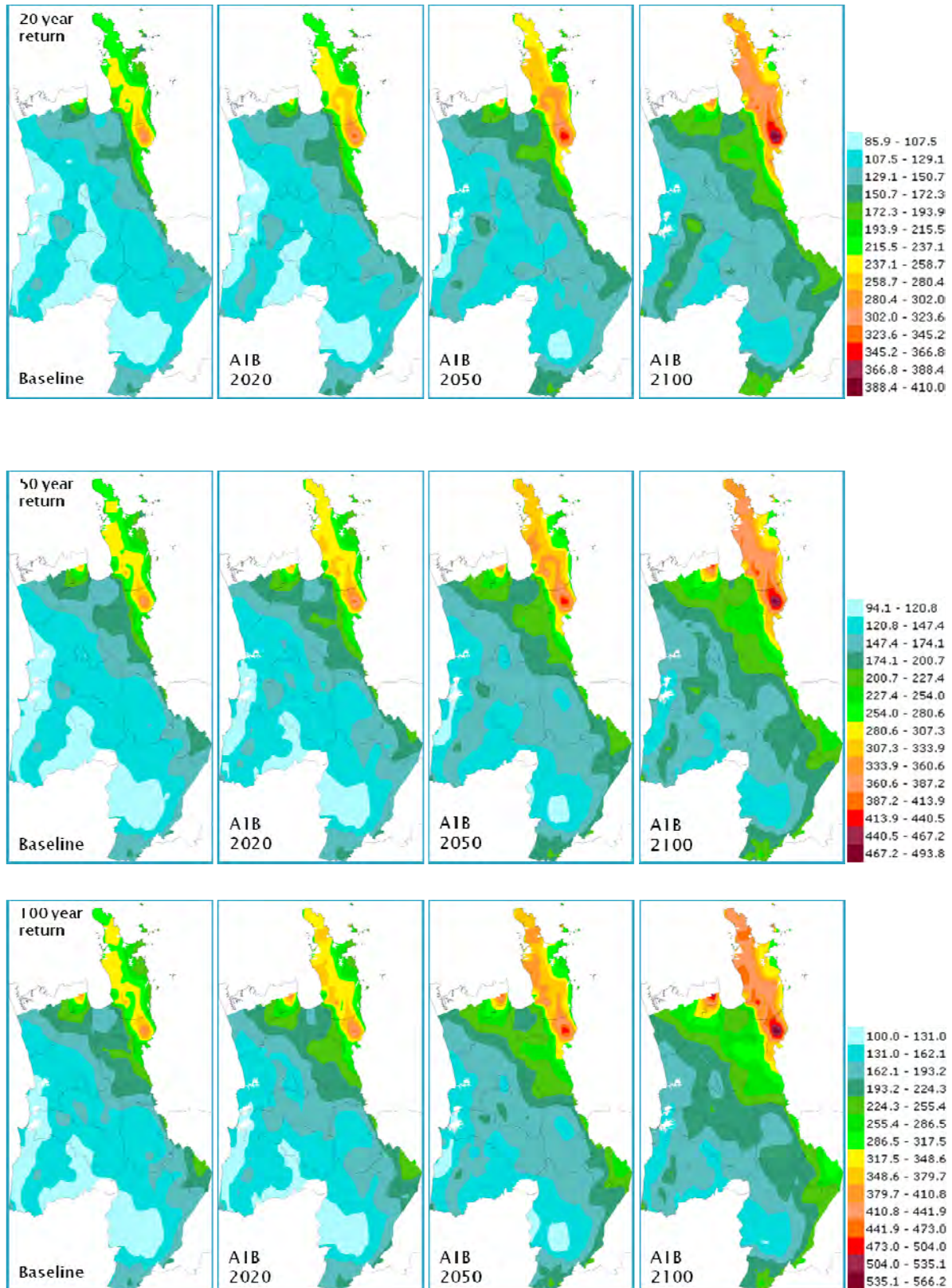
Figure 10. Extreme daily precipitation intensity (mm/day): Baseline and median projections for 20-year, 50-year and 100-year ARIs, for 2020, 2050, and 2100 (A1B, Median) scenarios.
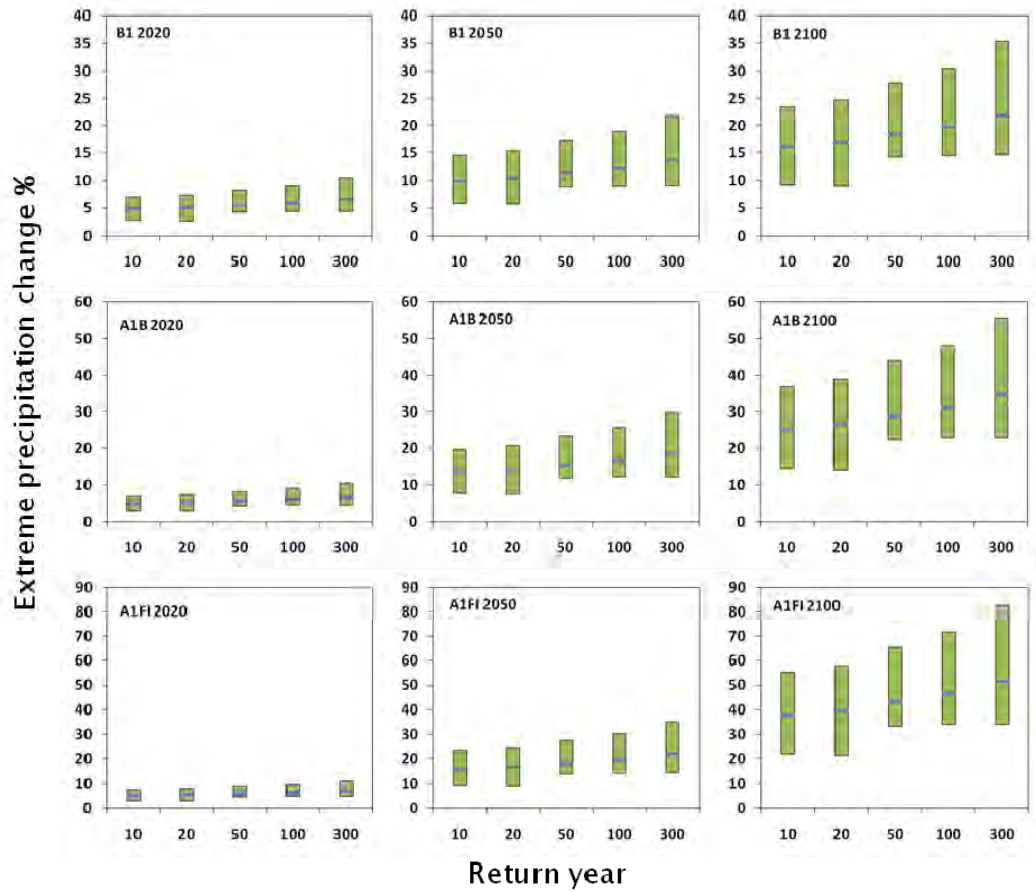
Figure 11. Extreme daily precipitation changes (percent change) for the Waikato region: B1 (top panel), A1B (middle) and A1FI (bottom panel), for 2020, 2050 and 2100 scenarios. Results from the 12-GCM ensemble, Low, Median and High percentiles represented by the green boxes.

Table 5 shows results of the analysis of extreme precipitation changes by 2050 (A1B), for the Thames-Coromandel district, given the higher values evident for this area relative to other parts of the Waikato region. Extreme precipitation is projected to increase by 14.2% for a 20-year ARI, by 15.48% for a 50-year ARI, and by 16.64% for a 100-year ARI (Median).

Table 5. Extreme daily precipitation change (mm/day) for the Thames-Coromandel District: Baseline and 2050 (A1B) change (percent change). Results from the 12-GCM ensemble: Low, Median and High percentiles.

ARI (year)	Baseline (mm/day)	Low %	Median %	High %
5	162.09	8.63	**13.38**	19.48
10	194.00	7.79	**13.56**	19.75
15	212.98	7.30	**13.86**	20.15
20	226.71	7.60	**14.20**	20.79
30	246.54	9.62	**14.76**	21.90
40	260.98	11.09	**15.17**	22.74
50	272.42	11.91	**15.48**	23.42
100	309.40	12.20	**16.64**	25.66
150	332.13	12.21	**17.46**	27.08
200	348.79	12.25	**18.03**	28.14
300	373.07	12.26	**18.47**	29.69

Extreme daily precipitation is projected to increase from 220mm/day (Baseline) to 250mm/day by 2050 (A1B) and to 280mm/day by 2100 (A1B) for a 20-year ARI for the Thames-Coromandel district. For a 100-year ARI, extreme precipitation increases from 305mm/day (Baseline) to 350mm/day by 2050 (A1B) and to 400mm/day by 2100 (A1B). Changes to the ARI values for a particular extreme daily precipitation intensity value (mm/day) can also be evaluated. For instance, an extreme daily precipitation value of 310mm/day with a 100-year ARI (Baseline) is projected to have an ARI of 45 years by 2050 (A1B) and an ARI of 28 by 2100 (A1B) (where the hashed line intersects with the A1B 2050 and A1B 2100 trend lines, respectively).
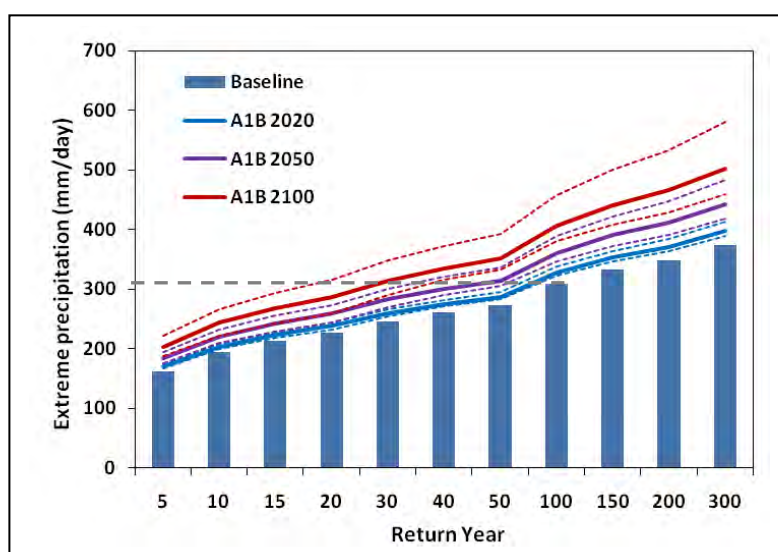
Figure 12. Changes in extreme daily precipitation (mm/day), for the Thames-Coromandel area. The blue bars indicate the baseline extreme precipitation values, and the coloured solid lines show the future projections of extreme precipitation per ARI using A1B: 2020 (blue), 2050 (purple) and 2100 (red) with corresponding coloured dashed lines representing the respective 10 and 90 percent confidence intervals.

2.2.4   Discussion and Conclusions

The analyses found that all 12 GCMs project an increasing trend in extreme daily precipitation for the Waikato region for 2020, 2050 and 2100 scenarios. This is a noticeable difference with mean annual precipitation change (where both decreases and increases were evident). This pattern is consistent with climatological theory (Emori and Brown, 2005; Cubasch et al., 2001; Trenberth, 1999). In this report the direct results from GCM extreme daily precipitation scenarios for the Waikato region were used. As a result, our values are higher than global mean in extreme daily precipitation percent change, which is approximately 8% per degree global warming (MfE, 2008).

The changes in extreme daily precipitation for the Waikato region are spatially variable, increasing between 10-13% (B1 and A1B) and 15-20% (A1FI) by 2050 and between 25-35% (A1B) and 38-52% by 2100, as shown in Figure 10. Changes by 2020 were less than this, with a median change of 5-7%. Therefore, by 2050 and 2100 the changes projected are higher than the global mean of 8% projected per degree global warming. This spatial variability in extreme daily precipitation change is characteristic of broader New Zealand trends reported (MfE, 2008).

Note: MfE (2008) suggest that even a 30-year run for a particular model is probably not long enough to get stable statistics of extreme precipitation events. **Therefore MfE recommends, that the same changes to rainfall return periods be applied everywhere across New Zealand.** The recommended adjustment factors are given in Table 5.2 of the MfE report, with an example in Appendix 4 (MfE, 2008). This recommendation should be taken into consideration, in assessing the above results.

2.3   Peak streamflow change

2.3.1   Introduction

Various studies report that as a result of climate change, heavier and/or more frequent extreme rainfall events are expected over New Zealand, especially in areas where the mean rainfall is projected to increase (MfE, 2010; IPCC, 2007b). The inter-annual variability in rainfall in particular, as well as extreme rainfalls that induce floods, are influenced by the ENSO (El Niño Southern Oscillation) patterns in the South Pacific region. The ENSO effect is expected to maintain its influence on regional climate, with extreme high rainfalls projected coincident with La Niña phases of the ENSO, and extreme low rainfall events coincident with El Niño phases of the ENSO (IPCC, 2007b). The percentage increase in extreme rainfall intensity is expected to be approximately 8% per degree global warming (Mullan et al., 2005). In this report, extreme stream flow at each ARI value was calculated using the General Extreme Value (GEV) distribution and the *L*-moments parameter estimation (Walpita-Gamage et al., 2009; Malamud and Turcotte, 2006).

2.3.2   Methodology and data

As described in MfE (2010), increases in extreme rainfall are expected to represent the major impact of climate change on New Zealand river floods, while in coastal river reaches, sea-level rise will also affect inundation. Due to the complexity of the hydrological relationship between rainfall intensity and peak flow, and the uncertainty of projections of precipitation change, this report uses a method that is most commonly in use and provides a simple Rational Method (MfE, 2010). The equation for the Rational Method is provided below (as per MfE, 2010) as:

Q = C i A /3.6

Where,
Q is an estimate of the peak design discharge in cubic metres per second (m^3/sec)
C is the run-off coefficient

i is the rainfall intensity in millimetres per hour for a duration equal to the time of concentration of the catchment, and
A is the catchment area in square kilometres

However, as MfE (2010) points out, the relationship between rainfall intensity and flood magnitude depends on several factors that do not have a linear relationship; such that, for example, an 8% increase in rainfall intensity may not result in an 8% increase in flood peak discharge, or subsequently an 8% increase in flood inundation. Therefore, understanding of rainfall–runoff inundation processes also need to be integrated in hydrological modelling efforts as these relate to an increase in rainfall.

The Rational Method is an empirical method to estimate peak flow. It is characterised by several features: rapid implementation, low data requirements, widely used in the engineering community, guidelines for estimating run-off coefficient are available. However, it is not suitable where rainfall varies significantly across the catchment, and it does show limited accuracy in validation tests. The Rational Method only needs rainfall intensity and run-off coefficients, which depend on catchment characteristics (i.e., slope, land cover, soil), the time of concentration and catchment area (MfE, 2010).

The future extreme peak flows were calculated using the flood estimate recommendations from MfE (2010). Changes to peak flows were projected using climate change scenarios for 2020, 2050 and 2100. The stations were chosen on the basis of having complete records for 30 or more years, as is standard methodology in climate change impact assessment (Martin and Parry, 1999). Two streamflow stations were selected to analyse historical streamflows in the Waikato region: (1) Kauaeranga station, on the Kauaeranga River, and (2) Te Aroha station, on the Waihou River. Both stations are located in the north-eastern part of the region in the Thames-Coromandel and Hauraki Districts, respectively (see Figure 13).
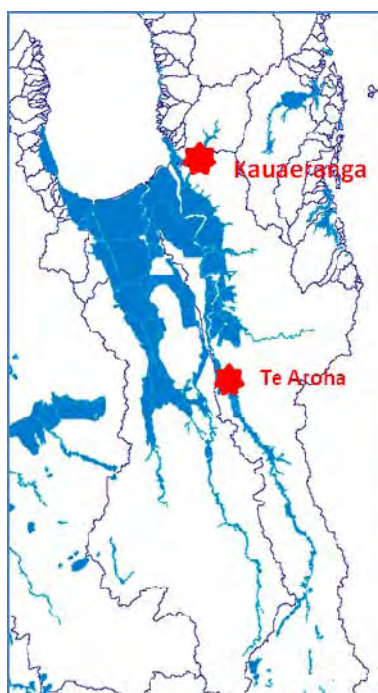
Figure 13. Map of the two streamflow stations used for the analysis of changes to extreme streamflow (Source: EW GIS layers).

2.3.3 Results

2.3.3.1 Baseline and future peak streamflows

The Thames-Coromandel and Hauraki Plains (where the two rivers traverse) are identified by Environment Wiakato as 'Risk Areas' prone to large flood events. The Thames-Coromandel has very steep and small catchments with short run-off distances to rivers and is an area that is susceptible to tropical storm activity, while the Hauraki Plains have low-lying farmland and towns along the Waihou and Piako river systems that are vulnerable to flooding (see http://www.ew.govt.nz/environmental-information/Regional-hazards-and-emergency-management/River-flooding/#Heading1).

For the Waihou River, using an ARI of 100 years, Figure 14 (top figure) shows that the peak flow volumes are projected to increase from ca 580m^3/sec to ca 700m^3/sec by 2050 (A1FI) and to ca 780m^3/sec by 2100 (A1B). An ARI of 50 years is projected to increase from ca 480m^3/sec to ca 550m^3/sec by 2050 (A1B) and to ca 630m^3/sec by 2100 (A1B). For the Kauaeranga River, for an ARI of 100 years, Figure 14 (bottom figure) shows that the peak flow volumes (m^3/sec) are projected to increase from ca 1150m^3/sec to ca 1370m^3/sec by 2050 (A1B) and to ca 1550m^3/sec by 2100 (A1B). An ARI of 50 years is projected to have increases in peak flow volumes from ca 1050m^3/sec to ca 1250m^3/sec by 2050 (A1B) and to ca 1400m^3/sec by 2100 (A1B).

The parallel dashed lines in Figure 14 show the change in ARIs over time. For example, an event with an ARI of 100 years in the baseline period is ca 580m^3/sec. This peak flow value of 580m^3/sec, intersects the A1B 2100 curve at an ARI of ca 40 years. This therefore projects that an event that has a current ARI of 100 years becomes an event with a projected ARI of 40 years by 2100 (A1B). Corresponding changes to other ARI values are also illustrated in Figure 14.
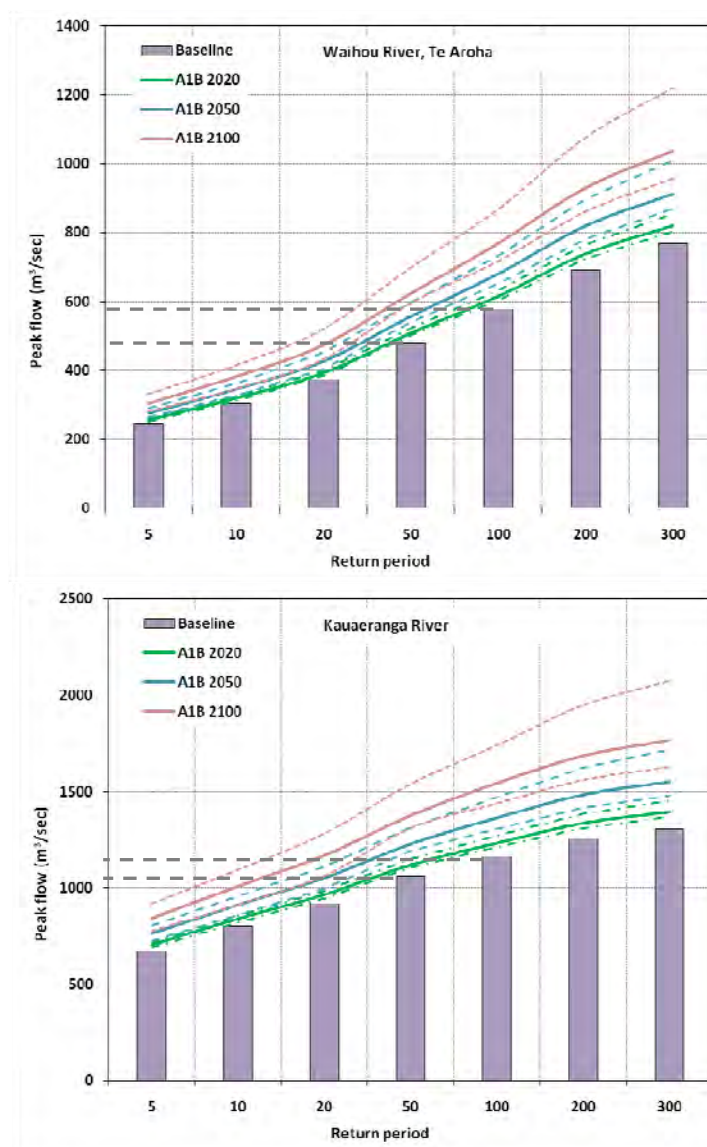
Figure 14. Peak flows (m3/sec) and corresponding ARI values for baseline and future climate change scenarios for the Waihou River, (station at Te Aroha) (top figure) and the Kauaeranga River (station at Kauaeranga station) (bottom figure) for 2020, 2050 and 2100 using A1B.

2.3.4   Discussion and Conclusions

Climate change is projected to increase projected extreme peak flow in rivers such as the Kauaeranaga River and the Waihou River of the Waikato region. Additionally, climate change is projected to decrease the ARIs for peak flows relative to the baseline period. This is consistent with the projections at the national level for New Zealand in studies such as those of MfE (2010). Note that the increase in extreme rainfall and peak flow events is despite the fact that in the same regions (Thames-Coromandel and Hauraki districts), the PED values are also projected to increase (refer to Section 2.4.3). This suggests that both extremes of flood- and drought-inducing climatic conditions are being projected for these areas.

Other streams and rivers in the Waikato region also can be assessed for the impact of climate change on peak flows, however, the ones that have been selected here are for areas that are already

known to be in hotspots of flood risk and therefore provide a relevant indicator of potential changes for the future.

2.4   Potential Evapotranspiration Deficit (PED)

2.4.1   Introduction

The majority of climate change scenarios, project decreases in precipitation for the eastern regions of New Zealand in the future, resulting in the eastern parts of the country experiencing more frequent drought events by the end of the 21st century, if greenhouse gas emissions continue to rise (Mullan et al., 2005). This has implications then, for the eastern parts of the Waikato region over the coming decades, and needs to be assessed for the extent and severity of the likely impacts. Drought occurrences affect agriculture and water resource management in particular, and the long-term planning for these sectors (Mullan et al., 2005; Jones, 2001).

2.4.2   Methodology and data

In order to compare the results produced in this Assessment with those of the national drought assessment (Mullan et al. 2005), the Potential Evapotranspiration Deficit (PED) was calculated for the baseline period (1972-2008), using the methodology in Mullan et al., 2005. Further details of the PED calculation are provided in Appendix 4.

Translating PED index values into drought severity thresholds that are applicable across the country is complicated, since a similar PED level in one region for which it is noted that farmers can adapt to, may cause adverse effects in other parts of the country that are accustomed to wetter conditions. For instance, in the drier eastern regions a PED of 200mm results in ca 1.5-2 months of water deficit, and 600mm to ca 5months. For pasture-based agricultural systems, this would mean that when PED>200mm, there are up to 2 months of the year when there is insufficient water available for pasture growth (assuming that there is no irrigation to ameliorate the effects of the water deficit).

A worst case scenario, when PED>200mm and PED>400mm, was calculated using the future scenarios for a combination of the High (90th percentile of the ensemble) of global temperature change and a Low (10th percentile of the ensemble) of global precipitation change (using A1FI). The rationale for this combination is to test, future climatic conditions with a high temperature increase and low precipitation increase that result in intense dry climatic conditions. The worst case combination is presented to reflect the full range of possible changes to PED, although this situation is less likely to occur.

2.4.3   Results

2.4.3.1 Baseline and future Potential Evapotranspiration Deficits

Figure 15 shows the percentage of years, over a 40 year virtual period, with values for PED>200mm. For 2020, 2050 and 2100 scenarios, the 40-year virtual period is taken as 2000-2039, 2030-2069 and 2080-2119, respectively.

The results indicate a 'hotspot' of PED in the north-eastern parts of the Waikato region, mainly on the border between the Hauraki and Thames-Coromandel districts and south into parts of the Matamata-Piako and Waikato districts by 2020 and 2050, intensifying by 2100. Additionally, parts of the South Waikato, Rotorua and Taupo districts show higher PED values by 2100. By 2050, between 72.2-90.3% of years in a 40-year period, centred around 2050, have a PED>200mm in the Hauraki district and parts of Thames-Coromandel district, which increases spatially by 2100. Table 7 provides percentage values for comparison.
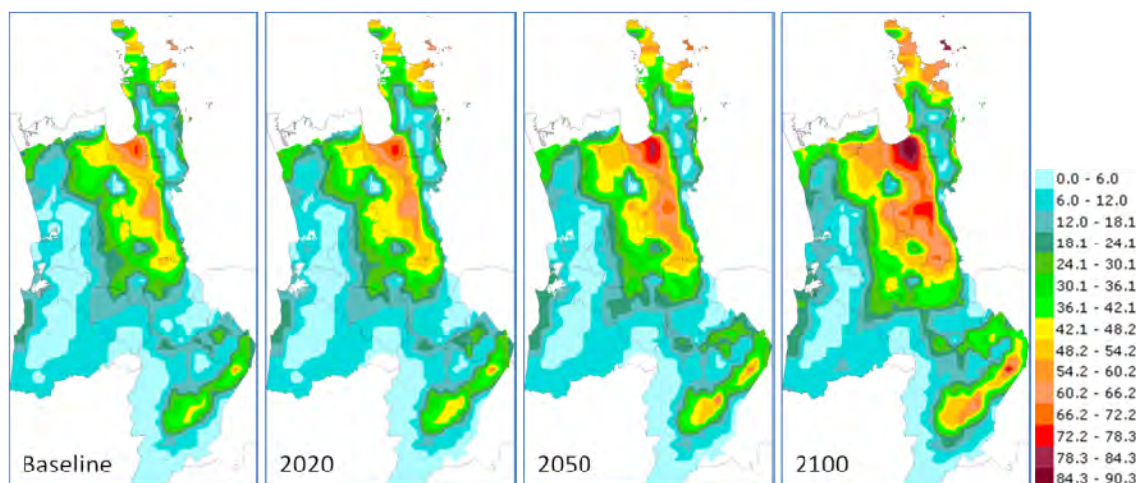
Figure 15. Percentage of annual PED by 2020, 2050 and 2100, where PED>200mm (A1B, Median). (The spatial change results for PED>400mm are minimal as evident in Table 6).

Table 6. Percentage of PED>200mm and PED>400mm during the baseline and under the A1B scenario.

	Low	Median	High
Baseline	18.12	PED>200	
A1B 2020	18.90	19.20	19.31
A1B 2050	20.40	21.38	22.20
A1B 2100	22.37	24.34	25.63
Baseline	0.25	PED>400	
A1B 2020	0.27	0.29	0.30
A1B 2050	0.36	0.43	0.46
A1B 2100	0.49	0.69	0.83

Figure 16 presents the worst case scenarios (A1FI) where PED>200mm and PED>400mm. For the baseline period, the occurrence of areas where PED>400mm is minimal (Figure 16, bottom panel). However, by 2050 and 2100 areas where PED>200mm and PED>400mm are projected to increase in spatial extent (Figure 16 top and bottom panels). Extensive parts of the Hauraki and Matamata-Piako districts experience up to 73.3-100% of years when PED>200mm, over a 40-year period centred around 2100. Franklin, Thames-Coromandel, South Waikato, Waikato, Waipa, Taupo and Rotorua districts also experience 73.3-100% of a 40-year period, centred around 2100, when PED>400mm. However, the effect is more restricted spatially than when PED>200mm.

Figure 17 shows the percentage change in PED>200mm and PED>400mm by 2020, 2050 and 2100. The occurrence of PED>200mm is projected to increase by ca 3.0% by 2050 (A1B and A1FI), ca 6.2%

centred around 2100 (A1B) and 8.3% centred around 2100 (A1FI); while the percentage change in occurrence of PED>400mm increase minimally by ca 0.19% by 2050 (A1B and A1FI), ca 0.43% by 2100 (A1B), and ca 0.72% by 2100 (A1FI).
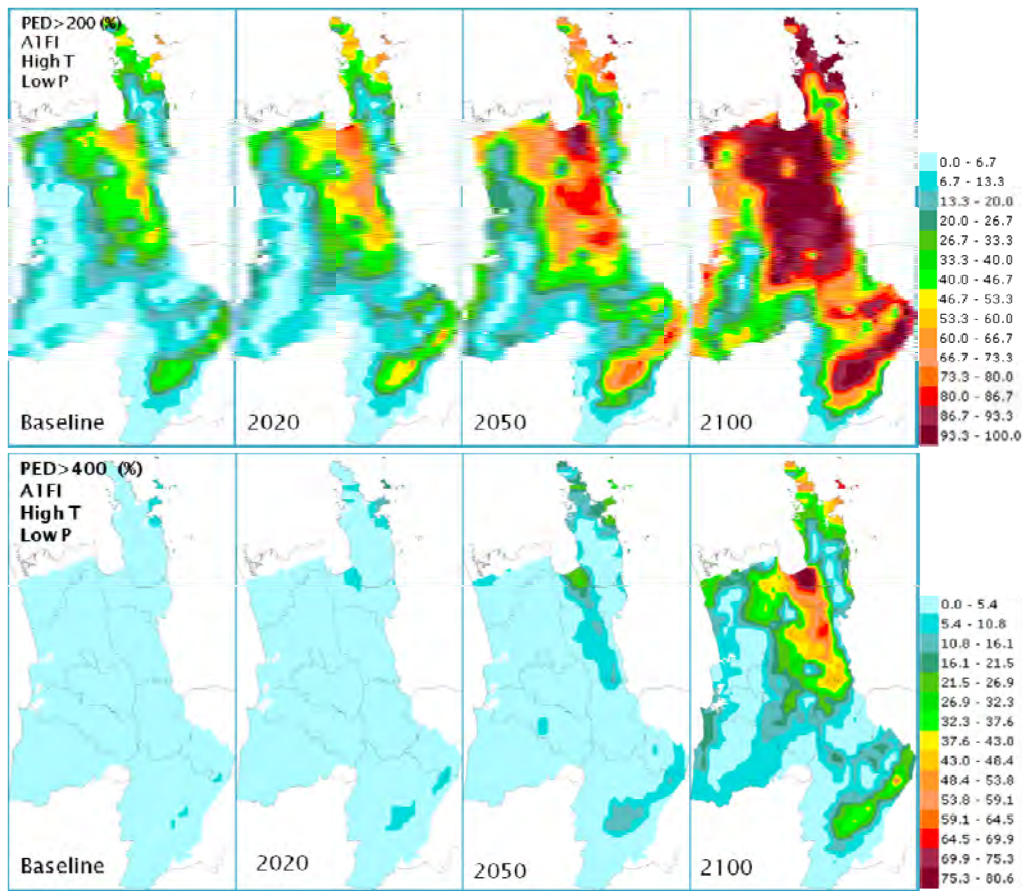
Figure 16. The worst case scenario for PED, combining a High (90th percentile) of GCMs for temperature change and Low (10th percentile) of GCMs for precipitation change (A1FI).
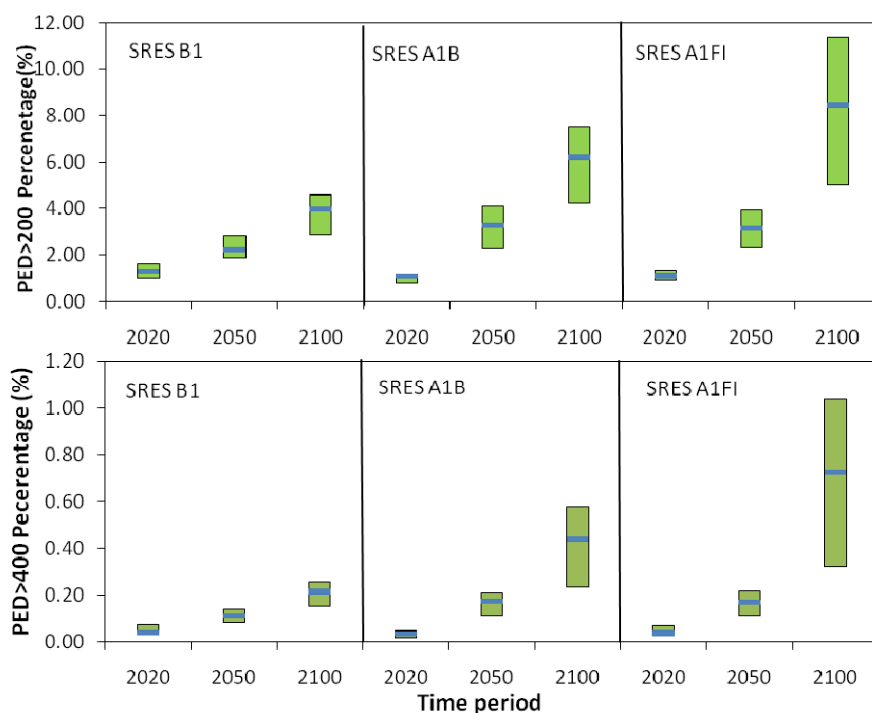
Figure 17. Percentage change in PED>200mm and PED>400mm: B1, A1B and A1FI for 2020, 2050 and 2100 for the Waikato region.

Figure 18 (top panel) shows the annual variation of PED for the baseline period for the Hauraki district. The July 2007–June 2008 period was the driest year in the time series, when the average PED was as high as 356mm (Median). The 2007/2008 summer-autumn was considered to represent a widespread drought event for most parts of the country, with the Waikato region incurring the highest dairy-related drought costs of $779 million (Butcher Partners Ltd, 2009). The lowest PED values for this time series were in 1983-1984, with a PED of 38.3mm (Median). The green bars indicate that the PED shows spatial variability across the Hauraki district, even though it is not a large district.

Figure 18 (bottom panel) illustrates changes in PED that have been perturbed to provide future change values by 2050 and 2100. The perturbation is also called a 'change factor', and involves adding the change factors of monthly mean changes for future scenarios to the historic observed daily data to form a new time series that represent the future climate conditions. For example, mean temperature in January is projected to increase by 1.2^{o}C by 2050 (A1B). Thus this 1.2^{o}C change factor is added to each day in January for every year in the time series. This time series becomes the representative time series centred around 2050 (A1B). By using this perturbed future time series, the future PED is calculated (Figure 18 (bottom panel)). Thirteen out of 36 years in the baseline period had values for PED>200mm. However, this is projected to increase up to 17 out of 36 years by 2100.
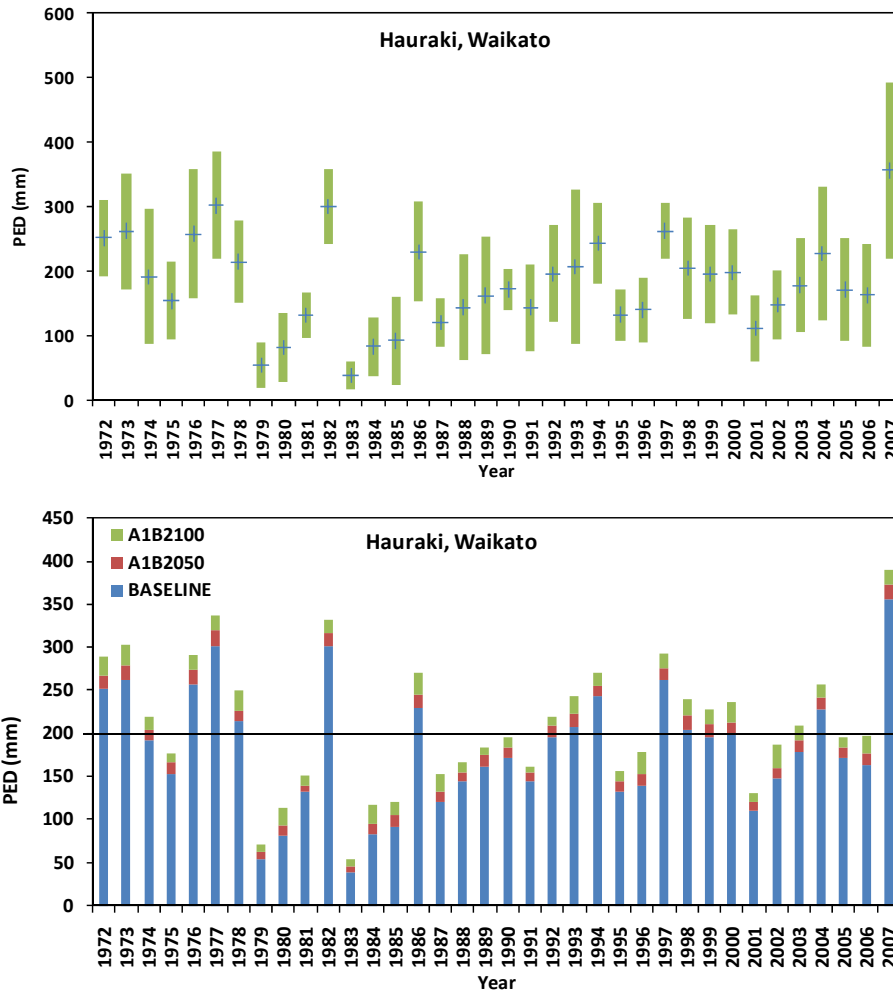
Figure 18. Annual variations in baseline PED (mm) (top panel) and the changes to PED (mm) with climate change (A1B for 2050 and 2100) (bottom panel) for the Hauraki district. The bars show the variations among years for the 49 PED spatial grid cells that cover the Hauraki district.

2.4.3 Discussion and Conclusions

PED is a useful index of the change in drought potential in the Waikato region under baseline and future scenarios. The spatial patterns produced in Figures 15 and 16 indicate that the projected hotspot of future drought exposure is in parts of the Hauraki district (up to 80% of years in a 40-year period centred around 2100 when PED>400mm), followed by the Matamata-Piako and Thames-Coromandel districts, (where localised areas have up to 65-70% of years in a 40-year period, centred around 2100, when PED>400mm) particularly by 2100.

Overall, under a high temperature increase and low precipitation increase scenario, the Waikato is projected to have significant areas that are exposed to PED>200mm from the mid-century onwards that could eventuate in increased drought risk and reduced water availability for pasture growth (up to 2 months per year likely). This intensifies by 2100 for parts of the Hauraki, Matamata-Piako and Coromandel districts (for PED>400mm that may result in 3-4 months of water deficit for pasture growth).

The spatial scenarios of PED change patterns are valuable in identifying areas with higher drought potential for regional planning purposes. However, PED values must be interpreted with regard to

other factors that increase or reduce drought vulnerability of human and ecological systems. Additionally, Mullan et al. (2005) suggest that it is easier to define an index such as the PED from a science perspective, than it is to ensure that this index is the most suitable one for the intended purpose. Hence they suggest that the limitations of a proposed index should be clear, and left open for ways in which it might be improved.

Mullan et al. (2005) notes that an index is needed that is appropriate for both national and regional analyses and that it should adequately cope with differing thresholds and scales of drought severity. It should also be suited for estimating drought risk for agricultural landscapes in New Zealand with associated agricultural production losses linked to both the duration and intensity of drought events. The descriptor of drought may need to include climatological and hydrological information, as well as information on crop and animal production performance and a soil moisture deficit related index, depending on whether one is describing meteorological drought, hydrologic drought or agronomic/agricultural drought (MAF, 2009)[4].

2.5   Temperature-Humidity Index (THI)

2.5.1   Introduction

The Temperature-Humidity Index (THI) is a measure that combines effects of high ambient temperatures and relative humidity. It is a useful index to assess the risk of heat stress to animals such as dairy and beef cattle in particular (Hahn et al., 2009; Bouraoui et al., 2002), though it is also applicable to human physiology and to other species and to. Studies have shown that dairy milk production and breeding efficiency of cows decrease with increasing thermal heat stress, for example, in Mediterranean climates (Bouraoui et al., 2002; Ingraham et al., 1975) and at extreme levels can endanger livestock (Hahn et al., 2009). However, other studies such as that of Dragovich (1979) highlight the fact that THI values need to be assessed in combination with other limiting factors. In general though, the THI index does capture much of the impact of warm to hot thermal environments on animals, by combining temperature and humidity parameters (Hahn, 2009).

2.5.2   Methodology and data

Details of the calculation of the THI used in this Assessment are shown in Appendix 6. The threshold values for THI are similar to those used by Dairy Australia, (under the programme 'Cool Cows: Dealing with heat stress in Australian dairy herds'. See also: de la Casa and Ravelo, 2003). The thresholds used for the THI are as follows:
1. If THI>72 (mild stress), cows are likely to begin experiencing heat stress and the in-calf rates will be affected;
2. If THI>78 (moderate stress), cows' milk production is seriously affected;
3. If THI>88 (severe stress), very significant losses in milk production are likely, cows show signs of severe stress and many ultimately die.

THI does not account for solar radiation or air movement. However, both of these factors along with air temperature and relative humidity will influence the heat exchange of the animals with their surroundings (Bouraoui et al., 2002).

---

[4] 1) <u>Meteorological drought:</u> the state of the climate system that creates abnormally dry weather, prolonged enough for the lack of rainfall to cause serious hydrological imbalances; 2) <u>Hydrologic drought:</u> A deficit of water in the landscape, either in ground water reserves or in the surface hydrological system such as rivers, streams, and lakes; and 3) <u>Agronomic/agricultural drought:</u> A protracted period of deficient precipitation resulting in extensive damage to crop/pasture growth and production (MAF, 2009).

2.5.3   Results

2.5.3.1 Baseline and Future Temperature Humidity Indices

The number of days with THI>72 (mild stress) and the number of days with THI>78, (moderate stress), for baseline and future 2020, 2050 and 2100 scenarios (using A1B) are shown in Figure 19. For the baseline period, the central parts of the Waikato region including Hauraki, Matamata-Piako, Waikato, Waipa and Otorohanga districts experience more days when THI>72, than the rest of the region. The highest number of days appears in the Hauraki district and parts of Matamata-Piako district, with between 56.5-64.6 days. However, by 2050, all the central areas of the Waikato region will have greater than 80 days when THI>72, and greater than 90 days when THI>72 in the Hauraki district and in parts of Matamata-Piako district. By 2100, large parts of the Waikato region experience 72>THI, with the largest number of days being located in the Hauraki, Matamata-Piako, Otorohanga, Waipa, Waikato and Thames-Coromandel districts.

With respect to the number of days when THI>78, Figure 19 (bottom panel) shows that this is negligible during the baseline period, such that there are no locations where the average number of days when THI>78 is more than 1 day. However, by 2050 (A1B), Matamata-Piako and Otorohanga districts are projected to have up to 4 days when THI>78, and by 2100, this increases to 8 days. Most parts of the central Waikato are projected to have between 4-8 days when THI>78 by 2100.

The average number of days when THI>72 is projected to increase to ca 15 days (B1), and 20 days (A1B and A1FI) by 2050 and up to 60 days (A1FI) by 2100 (Figure 20, top panel). The average number of days when THI>78 is projected to be minimal for 2020 and 2050 scenarios and increases by up to 3 days by 2100 (A1B) and by up to 4 days by 2100 (A1FI) (Figure 20, bottom panel). The green bars for 2100 scenarios for both THI>72 and THI>78 indicate, however, that there is a wide spread of projections by the individual GCMs, particularly under A1FI, which is a measure of the uncertainty associated with projections of THI by this time period.
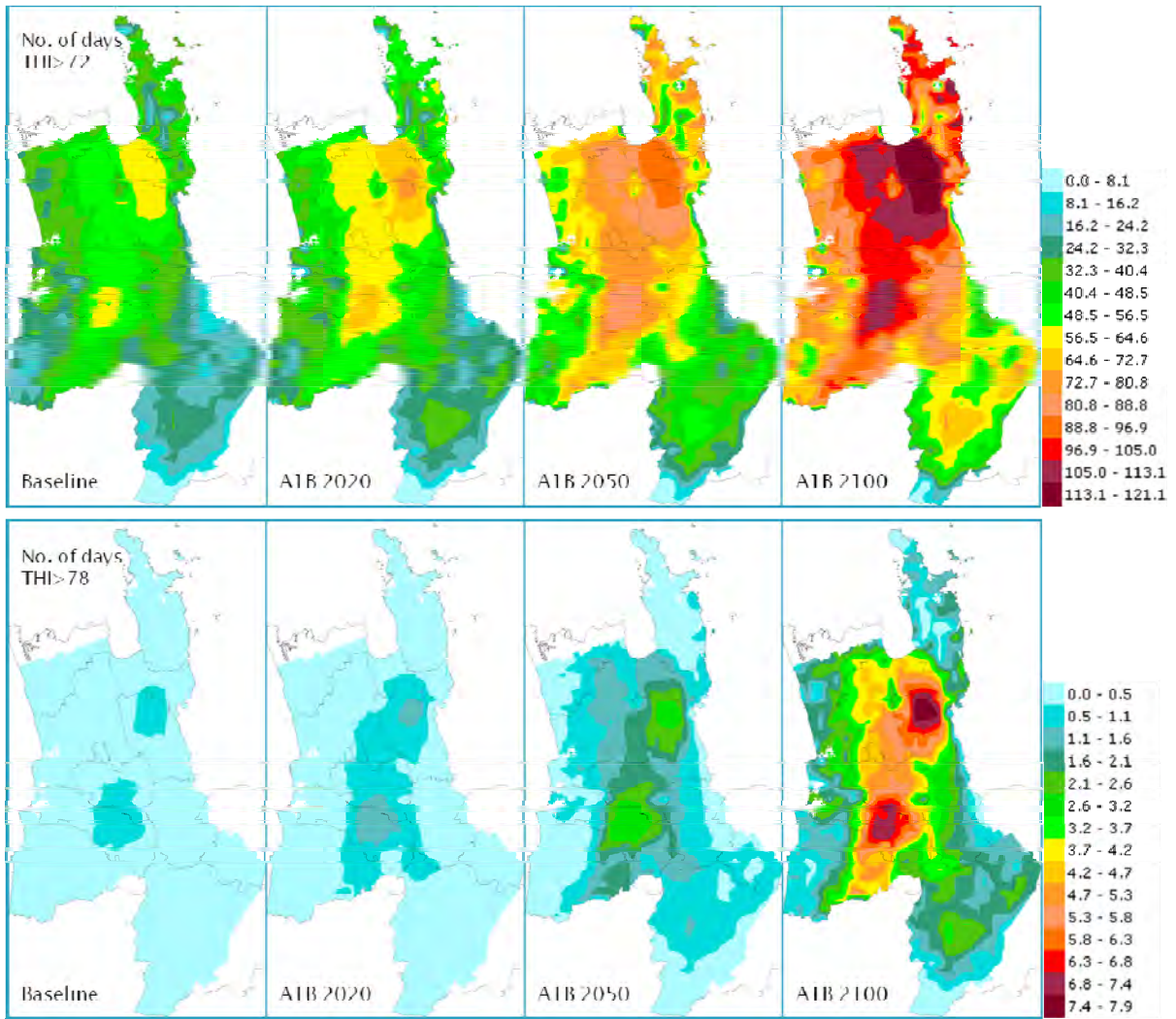
Figure 19. Number of days where conditions likely to induce mild stress (72<THI<78) (top panel) and moderate stress (79<THI<88) (bottom panel) to cattle, for baseline and future projections: A1B for 2020, 2050 and 2100 scenarios.
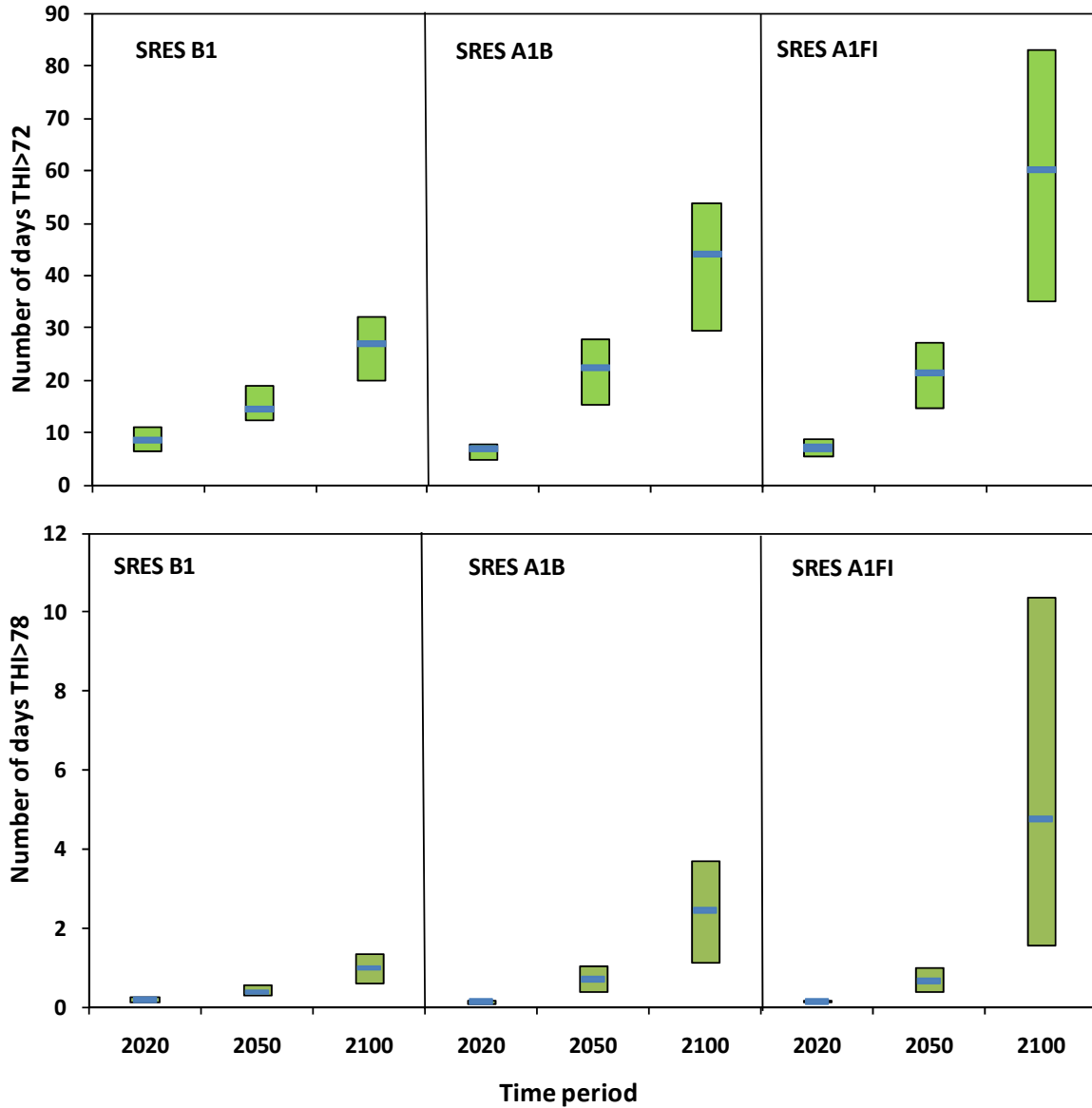
Figure 20. Change in average number of days per year when THI>72 (top panel) and THI>78 (bottom panel): B1, A1B and A1FI for 2020, 2050 and 2100 scenarios.

Further analysis was done focusing on the Hauraki district, using historical temperature records (1972-2008) for this area, given that it is one of the hotspots for higher THI values in the future. Figure 21 (top figure) shows that on average, there were about 50 days per year when 72<THI<78 for the baseline period of 1972-2008, and this increases to an average of 78 days by 2050 (A1B) and to an average of 99 days by 2100 (A1B). Figure 21 (bottom panel), shows a wide variation among years, and that on average there was about 1 day per year when 72<THI<78 was over the baseline period of 1972-2008. This increases to an average of 2-3 days by 2050 (A1B) and to an average of 7 days by 2010 (A1B).
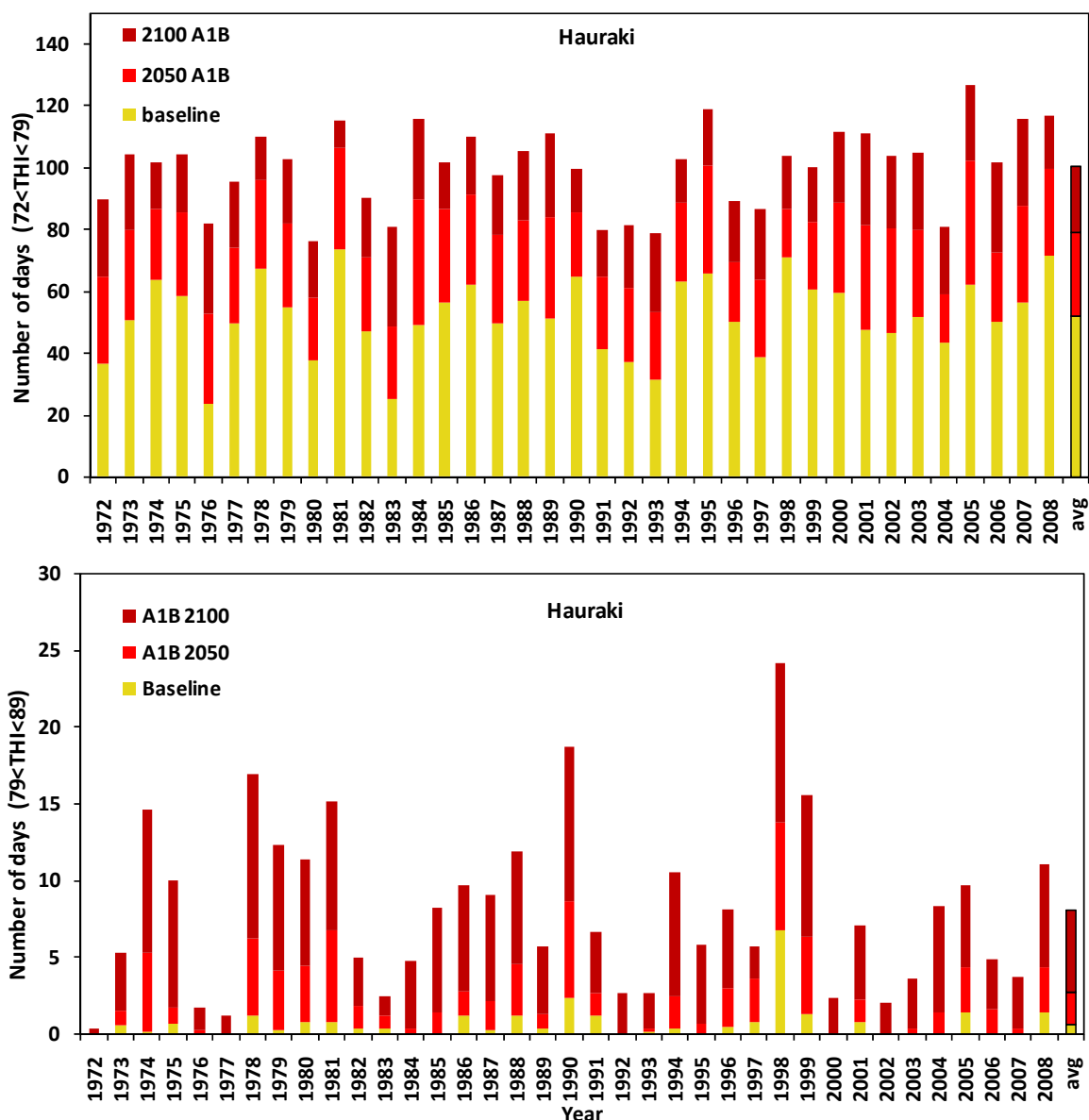
Figure 21. **Variations in number of days when 72<THI<79 (top figure) and 79<THI<89 (bottom figure) in the Hauraki District: for Baseline, 2050 and 2100 (A1B) scenarios.**

2.5.4   Discussion and Conclusions

THI scenarios for the Waikato region provide a useful indication of the changes to thermal heat stress projected by 2020, 2050 and 2100. The spatial patterns in Figure 19 illustrate that north-east and central parts of the Waikato region will be most affected by the intensifying THI values, particularly by 2050 and 2100. Similar to PED, the Hauraki and Matamata-Piako districts are a hotspot for increased THI values, along with parts of the Otorohanga district, and to a lesser degree parts of the Thames-Coromandel district. However, as Figure 20 shows, the scenarios for 2100 exhibit a wide range of modelled THI for individual GCMs in the ensemble (evident from the size of the green box by 2100), which is also a measure of the uncertainty associated with THI scenarios by that time horizon.

2.6   Growing Degree Days (GDD)

2.6.1   Introduction

Growing Degree Days (GDD) has been used as an effective measure of the amount of accumulated heat above a base temperature (at which growth processes are activated), to describe the length of the growing season and the timing of key lifecycle events for temperature-limited species (Kriticos et al., 2003; Ramankutty et al., 2002; Theurillat and Guisan, 2001; McMaster and Wilhelm, 1997). GDD can be used for both cultivated and wild species as well as species that pose a biosecurity risk to cultivation and biodiversity conservation. Conversely, GDD can also be used to identify areas where heat accumulation is insufficient, indicative of a cold stress influence on plant biological processes (Kriticos et al., 2003).

Various studies use GDD in combination with other climatic indices for applications such as: estimating field crop growing requirements (Basiden et al., 2008); estimating future species distribution changes with climate change (Kriticos et al., 2003); and changes in biosecurity disease risks (Sutherst, 1998) among others.

2.6.2   Methodology and data

There are various calculation methods in use for deriving GDD (Kriticos et al., 2003; Ramankutty et al., 2002; McMaster and Wilhelm, 1997). Here we use one of the more widely-used equations (McMaster and Wilhelm, 1997). To calculate GDDs for a site on a particular day, the daily mean temperature is calculated by averaging the maximum (highest) and minimum (lowest) temperatures for the day. Then a selected base temperature is subtracted from the mean temperature to get the number of GDDs for the 24-hour period. If the daily mean temperature is less than, or equal to the base temperature, the GDD value for that day is zero. This assumes that little or no growth takes place on those days.

The equation used to calculate GDD in this report is:

$$GDD = ((T_{max}-T_{min})/2)-T_{base}$$

2.6.3   Results

2.6.3.1 Baseline and future projections

GDD increases by ca $463.94^{o}D$ (A1B, Median) or $443.16^{o}D$ (A1FI, Median) by 2050; and ca $829.50^{o}D$ (A1B, Median) or $1058.31^{o}D$ (A1FI, Median) by 2100 for GDD>$0^{o}C$. The GDD values are much lower for GDD>$10^{o}C$ (A1B, Median), however the change relative to the baseline is ca $354.01^{o}D$ (A1B, Median) or $337.63^{o}D$ (A1FI, Median) by 2050 and ca $669.2^{o}D$ (A1B, Median) or $896.38^{o}D$ (A1FI, Median) by 2100. (These change values are calculated by subtracting the Baseline value from the future GDD projected value in Table 7). Figure 22 indicates the change in GDD above the three base temperatures, $0^{o}C$, $4^{o}C$ and $10^{o}C$.

Table 7. Regional average GDD for baseline and future scenarios: B1, A1B and A1FI for 2020, 2050 and 2100.

	>0°C GDD			>4°C GDD			>10°C GDD		
Baseline	**4766.15**			3312.56			1351.63		
	Low	Median	High	Low	Median	High	Low	Median	High
B1 2020	4884.41	4917.26	4972.75	3452.86	3489.62	3533.59	1461.88	1494.87	1534.72
B1 2050	5002.19	5054.47	5160.17	3554.57	3609.32	3699.89	1552.80	1589.07	1655.52
B1 2100	5172.20	5311.36	5391.25	3710.90	3841.62	3912.62	1665.81	1780.18	1848.26
A1B 2020	4859.13	4891.55	4906.72	3425.25	3461.08	3476.87	1437.65	1468.69	1482.72
A1B 2050	5067.16	**5230.09**	5321.69	3619.58	**3760.15**	3852.26	1597.15	**1705.64**	1789.02
A1B 2100	5347.88	**5595.65**	5753.04	3876.04	**4110.55**	4291.91	1809.44	**2020.83**	2154.06
A1FI 2020	4870.03	4896.19	4920.16	3437.27	3465.11	3490.95	1448.02	1472.76	1495.33
A1FI 2050	5061.66	5209.31	5310.78	3608.86	3740.25	3839.74	1590.50	1689.26	1778.48
A1FI 2100	5428.56	5824.46	6205.03	3956.40	4390.91	4742.04	1886.69	2248.01	2561.41
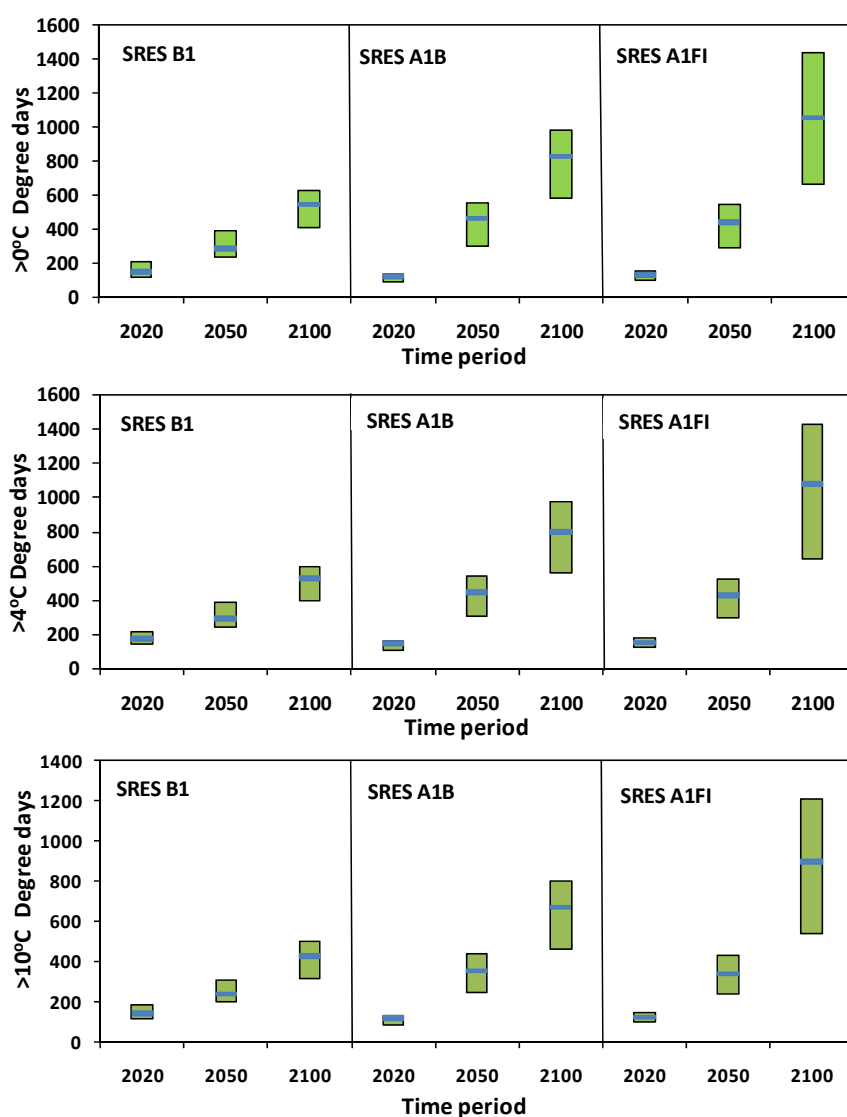
Figure 22. Change in average Growing Degree Days above three base temperatures 0°C, 4°C and 10°C for 2020, 2050 and 2100 (B1, A1B and A1FI) scenarios.

Figure 23 shows the baseline and future scenarios of the GDD using three alternative base temperatures: 0°C, 4°C and 10°C for 2020, 2050 and 2100 (A1B). The GDD values increase in the northern districts of the Waikato region by 2020, 2050 and 2100, particularly in the Thames-Coromandel, Hauraki, Matamata-Piako, Waikato and Franklin districts. GDD increases the most above the base temperature of 0°C by 2050 and 2100.
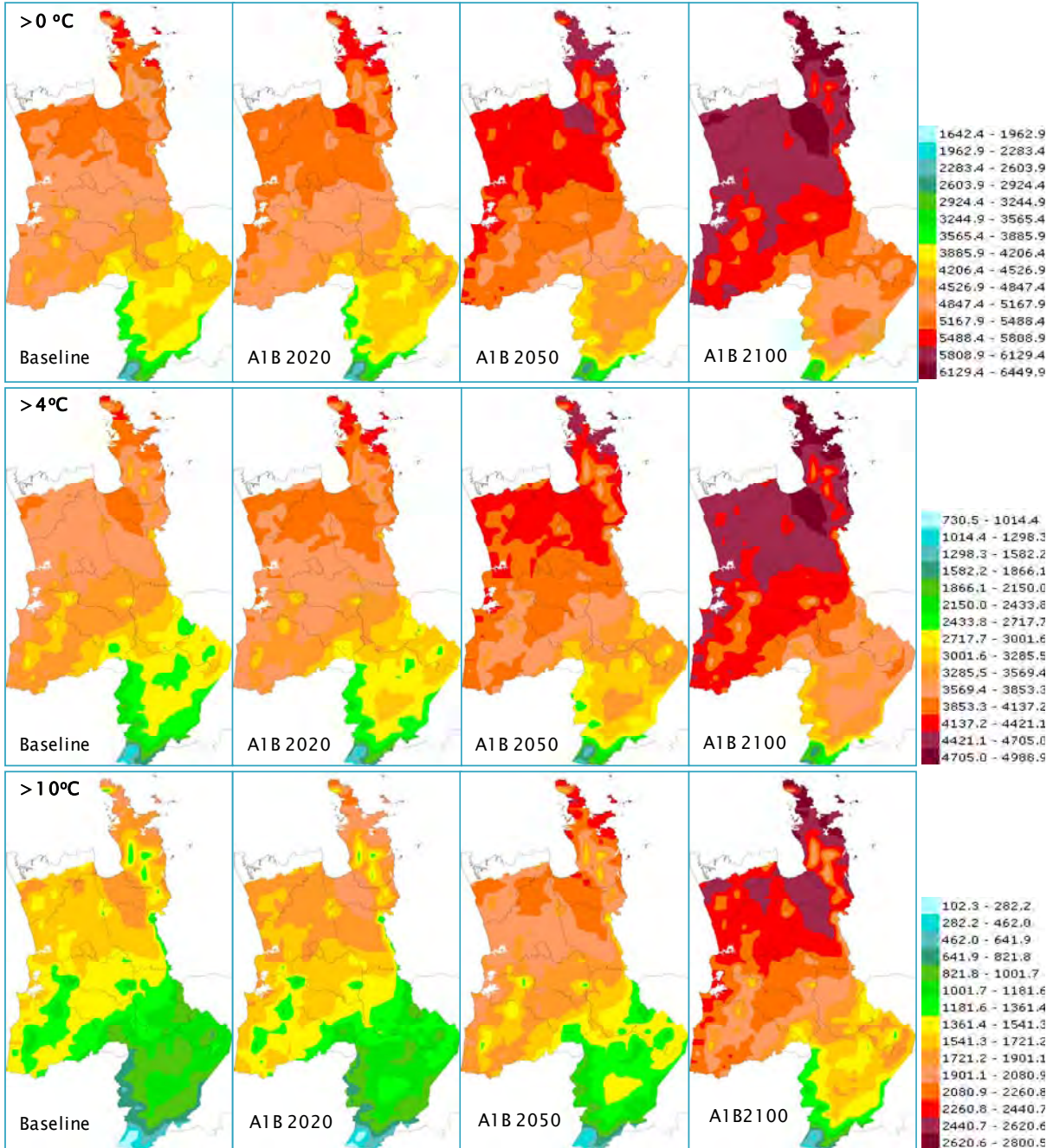
Figure 23. Growing Degree Days for base temperature >0°C, >4°C and >10°C: for baseline, 2020, 2050 and 2100 (A1B) scenarios.

2.6.3 Discussion and Conclusions

The GDD future scenarios for 2020, 2050 and 2100 indicate that there will be a lengthening of the growing season for the Waikato region for species that require base temperatures such as 0^oC, 4^oC and 10^oC to initiate growth. GDD increases by ca 463.94^oD by 2050 and by 829.50^oD by 2100 for GDD>0^oC (A1B and A1FI respectively); and the increase is about 669.20^oD (A1B) by 2050 or 896.38^oD (A1FI) by 2100 for GDD>10^oC.

These results are consistent with the IPCC projection of changes to GDD for the North Island of New Zealand of between 500-800 degree days by 2080 (using a base temperature of 5^oC) relative to the baseline period (IPCC, 2001). According to the MAF ECOCLIMATE report for New Zealand (Baisden et al., 2008), this increase in GDD may result in changes such as earlier start dates for pasture growth in late winter or spring. Overall, the changes indicated by GDD for the growing season provide a useful measure that indicates potential geographic shifts in agricultural productivity and seasonal growing patterns. These shifts must be interpreted in conjunction with other climate and production-related information for meaningful planning of adaptation options.

2.7 Sea level rise

2.7.1 Introduction

Sea level rise is projected to increase globally over the 21st century. The IPCC Fourth Assessment Report (AR4) has estimated that Mean Sea Level (MSL) rose by 1.7mm/year over the 20th century. This global average was exceeded between 1961-2003 (by 1.8mm), and between 1993-2003 (by 3.1mm). Future global sea level rise projections are for a rise of 0.18-0.59m by the decade 2090-2099 (mid-2090s) relative to the average sea level for a baseline period over 1980-1999 (IPCC, 2007a). However, the IPCC AR4 has not put an upper threshold on the amount of future sea level rise due to the considerable uncertainty associated with the potential contribution from melting in the West Antarctic and Greenland ice sheets over the 21st century) (IPCC, 2007a; MfE, 2008). As stated by MfE (2008), relative sea levels have risen by 0.16m on average over the last 100 years around New Zealand, which is comparable to global sea level rise over the same time period.

2.7.2 Methodology and data

The methodology used for generating the sea level rise scenarios follows that provided by the IPCC AR4 sea level data archive. For more information on the procedure see Appendix 6.

2.7.3 Results

2.7.3.1 Baseline and future scenarios of sea level rise

Figure 24 shows the global mean sea level rise scenarios to 2100 under 6 SRES emissions scenarios (A1B, A1FI, A1T, A2, B1 and B2). MSL rise is projected to be between 28cm (B1) and up to 43cm (A1FI), with an uncertainty range between 18cm–0.59cm.

The rate of sea level rise for the Waikato region is projected to be higher than the global total sea level rise projections by 2020, 2050 and 2100. Table 8 provides sea level rise projection for the Coromandel area. (Please note: the sea level rise projections for the western and eastern coasts of the Waikato region are similar, therefore, only this representative site is provided).
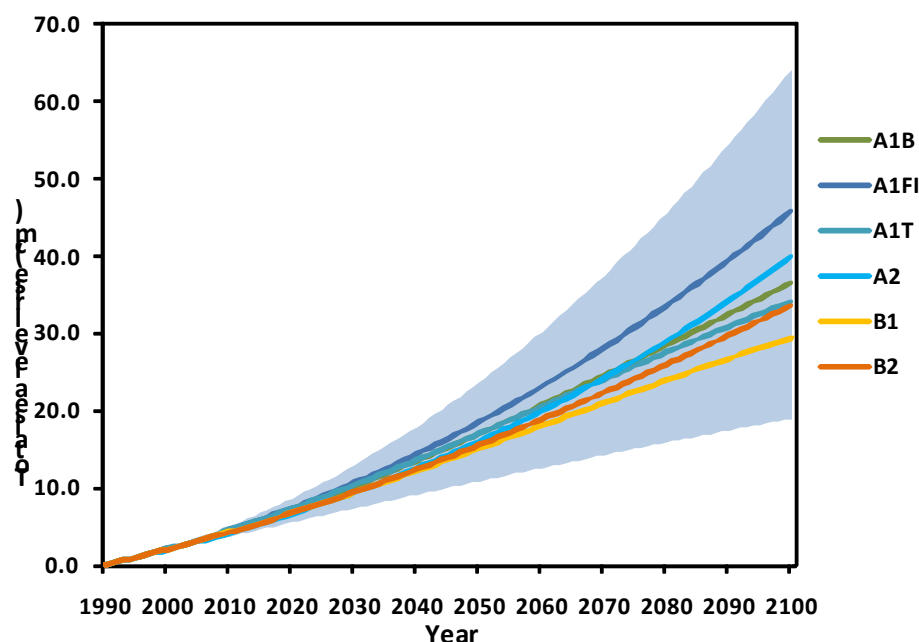
Figure 24. Global mean sea level rise generated from data published in IPCC AR4 WGI, Chapter 10, Table 10.7. This is without the scaled-up ice sheet discharge component, which is an alternative possibility of sea level rise (Meehl et al., 2007)[5].

Table 4 indicates that for the Coromandel area, sea level rise is projected to be 8.54cm (A1B, Medium) and 15.31cm (A1FI, High) by 2020 and up to 43.84cm (A1B, Medium) and 96.03cm (A1FI, High) by 2100. Sea level rise projected for the Coromandel is greater than the global mean sea level rise. However, these results do not take into account the localised variations in sea level rise projection that are possible, when vertical land movements are taken into account (due to land subsidence, sediment deposition and other geomorphic processes). Accurate data on vertical land movements for the Waikato region could not be accessed for this Assessment.

Table 8. Summary of sea level rise projections (cm) for Coromandel, Waikato.

	A1B	A1FI	A1T	A2	B1	B2
2020 Low	4.63	4.74	4.71	4.27	4.32	4.32
2020 Med	8.54	8.75	8.69	7.88	7.98	7.97
2020 High	14.95	**15.31**	15.20	13.80	13.97	13.94
2050 Low	11.02	11.98	11.04	10.38	9.75	10.03
2050 Med	20.34	22.12	20.39	19.16	18.00	18.52
2050 High	35.60	38.70	35.68	33.54	31.50	32.40
2100 Low	23.74	29.72	22.15	25.96	19.06	21.74
2100 Med	**43.84**	**54.88**	40.88	47.93	35.20	40.13
2100 High	76.71	**96.03**	71.55	83.87	61.59	70.22

---

[5] Scaled-up ice sheet discharge refers to the estimate of global sea level rise as a contribution from ice flows from the Antarctic and Greenland ice sheets (Meehl et al., 2007).

2.7.4. Discussion and Conclusions

The results show that the rate of sea level rise is projected to be higher for the Waikato region than at the global scale. This variation in the New Zealand trend, compared with the global trend is recognised by MfE (2008), which suggests that the reasons for these differences are not yet well-defined. In addition, it must be noted that the sea level rise projections in this Assessment for the Waikato region do not take into account the local variations in vertical land movements, which could modify the sea level rise values for specific locations. There is also uncertainty in higher sea levels, as a result of factors that are not currently included in the global climate models, on which projections are based (MfE, 2008).

In keeping with the national guidance in MfE 2008, we recommend that for medium- to long-term regional coastal planning purposes:

a. A base value sea-level rise of **0.5 m relative to the 1980–1999 average** should be used, along with

b. An assessment of the potential consequences from a range of possible higher sea-level rises, all assessments should consider the consequences of a mean sea-level rise **of at least 0.8 m** relative to the 1980–1999 average.

MfE 2008 also suggests that for planning and decision timeframes beyond 2100, where particular decisions taken have the potential to restrict future adaptation options, an allowance for sea-level rise of **10 mm per year beyond 2100** is recommended (in addition to the above recommendation).

3. Conclusions

This report provides an assessment of the key climate change impacts on the Waikato region in terms of projected changes by 2020, 2050 and 2100, for eight climatic indices:

1. Mean temperature change
2. Mean precipitation change
3. Extreme precipitation change
4. Peak streamflow change
5. Potential Evapotranspiration Deficit (PED)
6. Temperature-Humidity Index (THI)
7. Growing Degree Days (GDD)
8. Sea level rise

Additionally, this report provides detailed spatial scenarios for all of the listed variables except peak streamflow change and sea level rise (when site specific projections are provided). The Assessment provides information that is relevant to medium- and long-term spatial planning for the regional and district councils.

The results provided indicate that mean annual temperature increases by $1.20^{o}C$ by 2050 and by $2.18^{o}C$ by 2100 (under the A1B scenario). Summer (DJF) annual mean temperature increase is the highest seasonal change, $1.29^{o}C$ by 2050 (A1B) and by up to $2.45^{o}C$ by 2100 (A1B).

Mean annual precipitation change is highly variable, with both increases and decreases projected depending on the GCM used. This variability in the mean annual and seasonal precipitation projections (including the direction and magnitude of changes) indicates the inherent uncertainty associated with projections of precipitation change. The range of projected values is between a decrease of 6.15% and in increase of 6.08% by 2050 (A1B) and between a decrease of 11.57% and an increase of 11.35% by 2100 (A1B). Seasonal mean precipitation changes include projections for

winter (JJA) mean precipitation change of between -2.77% and 7.34% by 2050 (A1B) and between -5.19 and 13.75% by 2100 (A1B). Summer (DJF) mean precipitation is projected to change between -6.74 and 7.09% by 2050 (A1B) and between -12.58 and 13.18% by 2100 (A1B). The highest mean precipitation changes are projected for the Waitomo, Otorohanga, South Waikato and Taupo districts.

Extreme daily precipitation changes indicate an increase that is consistently located in north-east parts of the Waikato region – i.e. in the Hauraki and Thames-Coromandel districts and part of the Franklin district, despite projections for a decrease in annual mean precipitation by 2050 for these areas.

Peak streamflow changes are expected to increase in rivers such as the Kauaeranga and Waihou rivers which were selected for further analysis on the basis that extreme precipitation increases were also projected to be highest in the areas through which these rivers flow. The Average Recurrence intervals (ARIs) for peak streamflows are also expected to decrease (i.e. peak streamflows of specific values occur more frequently), and are described further in this report.

Projections for changes to PED also highlight the spatial variability of impacts with the highest PED values (where PED>400mm) located in the Hauraki and Matamata-Piako districts by 2100 (A1FI combining high temperature change and low precipitation change scenarios). However, PED>200mm (A1FI, combining high temperature and low precipitation scenarios) are more widespread across the Waikato region by 2050 and 2100, such that there will be an impact on most of the central, northern and eastern parts.

The THI index indicates that mildly stress-inducing conditions (THI>72) for animals such as dairy cows are widespread across the Waikato region by 2050 and more so by 2100. Moderately stress-inducing conditions (THI>78) are more restricted to the central parts of the Waikato region by 2050 and 2100, with two 'hotspots' evident in the Hauraki and Matamata-Piako districts and further south in the Otorohanga district, particularly by 2100.

GDD projections indicate that a lengthening of the growing season is expected across the entire Waikato region, although the increase is spatially variable and highest in northern districts where temperatures are warmer and lowest in the Taupo district. This projected lengthening of the growing season is likely to have beneficial effects on pasture and crop productivity in itself, and may create opportunities for new commercial crops to be cultivated. This increase in GDD also may have an impact on native species or species of importance to biosecurity, where GDD changes are likely to induce more favourable growing conditions. However, the increase in GDD also should be assessed in conjunction with changes to other climatological indices that affect crop production and species distribution, given that areas that have the highest GDD increases also have the highest PED and THI values.

Particular attention needs to be given to the Hauraki and Thames-Coromandel districts, which are identified as hotspots of potential drought and flood-related impacts.

The uncertainties associated with the future projections of the 9 climatic variables increase progressively between 2020 and 2100 scenarios, including uncertainties associated with future GHG emissions profiles, the earth's climate sensitivity to the GHG emissions, the extent of the effects of feedbacks mechanisms which may influence the rate and magnitude of climate change (IPCC, 2007a). The uncertainty has been represented in this Assessment by illustrating the spread of individual GCM projections within the various ensemble results.

On the basis of these patterns, we provide the following recommendations for more in-depth impacts assessments that will inform adaptation options and processes for the Waikato region.

4. Recommendations and future research direction

Recommendation 1:
It is important for baseline and future climate change projections of the Waikato region to be integrated into Regional Council strategies including those for hazard management, biodiversity and biosecurity management, coastal area management, water and land management and regional planning. This will assist in mainstreaming climate change effects into Regional Council policy.

Recommendation 2:
The north-eastern areas represent a 'hotspot' of potential increased flood occurrence due to increases in extreme daily precipitation into the future. This warrants further localised and more detailed assessment using hydrological modelling approaches to assess flood risk with future climate change. For a comprehensive perspective of the vulnerability of communities and infrastructure to these risks, socio-economic and land-use related variables will need to be integrated in the scenarios.

Recommendation 3:
Drought-inducing conditions in the Waikato region, estimated using the Potential Evapotranspiration Deficit (PED) index, will increase into the future for a considerable part of the Waikato region, particularly in the Hauraki and Matamata-Piako districts. Given the dependence of the regional economy on agricultural pasture, crop and animal productivity, this warrants a more in-depth assessment of drought risk that climate change poses. In addition, drought risk needs to be integrated with other climatological and hydrological information, and information on agricultural productivity (as suggested by MAF, 2008).

Recommendation 4:
Decreasing soil moisture availability, extent of streamflows and drought frequency and duration will have implications for water management. Thresholds for water scarcity for natural and managed systems will therefore need to be assessed and integrated in regional land-use scenarios to evaluate the level of risks into the future.

Recommendation 5:
Moderate heat-stress conditions (dairy cows used as an example in this report) likely will increase into the future, particularly in the central districts, as indicated by the Temperature-Humidity Index (THI). It is therefore important to assess in greater detail the implications of thermal heat stress on animal welfare by integrating climate change and information on animal physiology. This would then form the basis for addressing adaptation options for reducing animal stress (e.g., shade protection, dietary modifications).

Recommendation 6:
The Hauraki, Thames-Coromandel, Matamata-Piako and parts of Franklin districts are all identified as having the highest risk of exposure to extreme climatic events into the future in terms of precipitation. Therefore it is recommended that thresholds be determined for the likely implications of changing habitat conditions and ecosystem dynamics. A particular focus on the Significant Natural Areas (SNAs) located in the Hauraki district and surrounding areas is recommended.

Recommendation 7:
The future projected rate of sea level rise for the Waikato region is higher than the global total sea level rise projections. This will have implications for planning and decision-making with regard to future infrastructure, zoning development, socio-economic impacts and coastal ecosystems. Adaptation options need to be integrated into Regional Council policies that will accommodate strategies to cope with different thresholds of sea-level rise. Assessment is required of the implications of sea level rise together with baseline and future changes in other interacting variables in the coastal environment. These include Sea Surface Temperatures (SSTs), near-shore salinity, sedimentation, and the interactions of these on near-shore marine ecosystems and aquaculture.

4.   References

(Includes references listed in the Appendices).

Alexander, L. V., & Arblaster, J. M. (2009). Assessing trends in observed and modelled climate extremes over Australia in relation to future projections. *International Journal of Climatology, 29*(3), 417-435. 10.1002/joc.1730

Baisden, T., Greenhalgh, S., Kerr, S., Newton, P., Renwick, J., Stroombergen, A., et al. (2008). *Costs and benefits of climate change and adaptation to climate change in New Zealand: what do we know so far?* : Ministry for the Environment (MfE).

Benestad, R. E. (2002). Empirically downscaled temperature scenarios for northern Europe based on a multi-model ensemble. *Climate Research, 21*(2), 105-125.

Bouraoui, R., Lahmar, M., Majdoub, A., Djemali, M., & Belyea, R. (2002). The relationship of temperature-humidity index with milk production of dairy cows in a Mediterranean climate. *Animal Research, 51*(6), 479-491.

Brito-Castillo, L., Douglas, A. V., Leyva-Contreras, A., & Lluch-Belda, D. (2003). The effect of large-scale circulation on precipitation and streamflow in the Gulf of California continental watershed. *International Journal of Climatology, 23*(7), 751-768. 10.1002/joc.913

Butcher Partners Ltd. (2009). *Regional and national impacts of the 2007-2009 drought*: Prepared for MAF Policy by Butcher Partners Ltd. July 2009.

Carter, T. R., La Rovere, E. L., Jones, R. N., Leemans, R., Mearns, L. O., Nakicenovic, N., et al. (2001). Developing and Applying Scenarios. In *IPCC, 2001: Climate Change 2001: Impacts, Adaptation, and Vulnerability. CUP, Cambridge, UK.*

Cubasch, U., G. A. Meehl, G. J. Boer, R., J. Stouffer, M. Dix, A. Noda, et al. (2001). Projections of future climate change, in Climate Change 2001: The Scientific Basis. In E. J. T. Houghton et al. (Ed.), (pp. pp. 525-582,): Cambridge Univ. Press, New York.

Dai, A. (2006). Precipitation Characteristics in Eighteen Coupled Climate Models. *Journal of Climate, 19*(18), 4605-4630. doi:10.1175/JCLI3884.1

Dai, A., Trenberth, K. E., & Qian, T. (2004). A Global Dataset of Palmer Drought Severity Index for 1870-2002: Relationship with Soil Moisture and Effects of Surface Warming. *Journal of Hydrometeorology, 5*(6), 1117-1130.

de la Casa, A. C., & Ravelo, A. C. (2003). Assessing temperature and humidity conditions for dairy cattle in Córdoba, Argentina. *International Journal of Biometeorology, 48*(1), 6-9. 10.1007/s00484-003-0179-x

Dragovich, D. (1979). Effect of high temperature-humidity conditions on milk production of dairy herds grazed on farms in a pasture-based feed system. *International Journal of Biometeorology, 23*(1), 15-20. 10.1007/bf01553373

Emori, S., & Brown, S. J. (2005). Dynamic and thermodynamic changes in mean and extreme precipitation under changed climate. *Geophys. Res. Lett., 32*(17), L17706. 10.1029/2005gl023272

Hahn, G. L., Gaughan, J. B., Mader, T. L., & Eigenberg, R. A. (2009). Thermal indices and their applications for livestock environments. In *Livestock Energetics and Thermal Environmental Management. Chapter 5* (pp. pp. 113-130).

Hromadka Ii, T. V. (1989). The rational method in stormwater management modelling of peak flow flood control systems, I: Theoretical development. *Environmental Software, 4*(3), 123-129.

IPCC. (2000). *Emissions Scenarios. A Special Report of Working Group II of the Intergovernmental Panel on Climate Change.* Cambridge: Cambridge University Press.

IPCC. (2007a). *Climate Change 2007: The Physical Science Basis. Contribution of Working Group I to the Fourth Assessment Report of the Intergovernmental Panel on Climate Change* Cambridge, United Kingdom and New York, NY, USA.: Cambridge University Press.

IPCC. (2007b). *Climate Change 2007: Impacts, Adaptation and Vulnerability. Contribution of Working Group II to the Fourth Assessment Report of the Intergovernmental Panel on Climate Change*. Cambridge: Cambridge University Press, UK.

Jones, R. N. (2010). *A risk management approach to climate change adaptation, in: New Zealand Climate Change Centre 2010.Climate change adaptation in New Zealand: Future scenarios and some sectoral perspectives.* , Wellington.

Kharin, V. V., Zwiers, F. W., Zhang, X., & Hegerl, G. C. (2007). Changes in Temperature and Precipitation Extremes in the IPCC Ensemble of Global Coupled Model Simulations. *Journal of Climate, 20*(8), 1419-1444. doi:10.1175/JCLI4066.1

Kiktev, D., Caesar, J., Alexander, L. V., Shiogama, H., & Collier, M. (2007). Comparison of observed and multimodeled trends in annual extremes of temperature and precipitation. *Geophys. Res. Lett., 34*(10), L10702. 10.1029/2007gl029539

Kriticos, D. J., Sutherst, R. W., Brown, J. R., Adkins, S. W., & Maywald, G. F. (2003). Climate change and the potential distribution of an invasive alien plant: Acacia nilotica ssp. indica in Australia. *Journal of Applied Ecology, 40*(1), 111-124. 10.1046/j.1365-2664.2003.00777.x

Li Y., and Ye W. (2009). Applicability of ensemble pattern scaling method on precipitation intensity indices at regional scale, (submitted to *International Journal of Climatology*).

Lu, X., & Hulme, M. (2002). A Short Note on Scaling GCM Climate Response Patterns. Prepared for the AIACC regional study teams. June 2002. http://www.aiaccproject.org/resources/GCM/GCM.html

MAF. (2009). Drought Guide: Drought definition, recognition and assistance measures. From http://www.maf.govt.nz/mafnet/rural-nz/adverse-events/droughts/drought-guide.htm

Malamud, B. D., & Turcotte, D. L. (2006). The applicability of power-law frequency statistics to floods. *Journal of Hydrology, 322*(1-4), 168-180.

Malamud, B. D., & Turcotte, D. L. (2006). The applicability of power-law frequency statistics to floods. *Journal of Hydrology, 322*(1-4), 168-180.

Mayer, D. G., Davison, T. M., McGowan, M. R., Young, B. A., Matschoss, A. L., Hall, A. B., et al. (1999). Extent and economic effect of heat loads on dairy cattle production in Australia. *Australian Veterinary Journal, 77*(12), 804-808. 10.1111/j.1751-0813.1999.tb12950.x

McMaster, G. S., & Wilhelm, W. W. (1997). Growing degree-days: one equation, two interpretations. *Agricultural and Forest Meteorology, 87*(4), 291-300.

Meehl GA, S. T., Collins WD, Friedlingstein P, Gaye AT, Gregory JM, Kitoh A, Knutti R, Murphy JM, Noda A, Raper SCB, Watterson IG, Weaver AJ and Zhao Z-C. . (2007). Global climate projections. In Climate Change 2007: The physical science basis. Contribution of Working Group I to the Fourth Assessment Report of the Intergovernmental Panel on Climate Change In S. Solomon, D. Qin, M. Manning, Z. Chen, M. Marquis, K. B. Averyt, T. M. & & M. (Eds.) (Eds.): Cambridge, UK and New York, NY: Cambridge University Press.

MfE. (2008). *Climate Change Effects and Impacts Assessment: A Guidance Manual for Local Government in New Zealand. 2nd Edition.* : Ministry for the Environment, Wellington.

MfE. (2010). *Tools for estimating the effects of climate change on flood flow: A guidance manual for local government in New Zealand*: Prepared for Ministry for the Environment.

Min, S.-K., Simonis, D., & Hense, A. (2007). Probabilistic climate change predictions applying Bayesian model averaging. *Philosophical Transactions of the Royal Society A: Mathematical, Physical and Engineering Sciences, 365*(1857), 2103-2116. 10.1098/rsta.2007.2070

Mitchell, T. D. (2001). *An investigation of the pattern scaling technique for describing future climates.*, University of East Anglia, Norwich.

Mitchell, T. D. (2003). Pattern Scaling: An Examination of the Accuracy of the Technique for Describing Future Climates. *Climatic Change, 60*(3), 217-242. 10.1023/a:1026035305597

Mullan, A. B., Wratt, D. S., & Renwick, J. A. (2001). Transient model scenarios of climate changes for New Zealand. *Weather and Climate 21* 3-43.

Mullan B, Porteous A, Wratt D, & M, H. (2005). *Changes in drought risk with climate change*: Prepared for Ministry for the Environment (NZ Climate Change Office) and Ministry of Agriculture and Forestry.

Mullan, B., & Dean, S. (2009). *AR4 climate model validation and scenarios for New Zealand. Extended Abstract*. Paper presented at the 9th International Conference on Southern Hemisphere Meteorology and Oceanography.

Murphy, J. M., Booth, B. B. B., Collins, M., Harris, G. R., Sexton, D. M. H., & Webb, M. J. (2007). A methodology for probabilistic predictions of regional climate change from perturbed physics ensembles. *Philosophical Transactions of the Royal Society A: Mathematical, Physical and Engineering Sciences, 365*(1857), 1993-2028. 10.1098/rsta.2007.2077

Murphy, J. M., Sexton, D. M. H., Barnett, D. N., Jones, G. S., Webb, M. J., Collins, M., et al. (2004). Quantification of modelling uncertainties in a large ensemble of climate change simulations. *Nature, 430*(7001), 768-772.

Parry, M., & Carter, T. (1998). *Climate Impact and Adaptation Assessment*. London, UK: Earthscan Publications Ltd.

Patz, J. A., Campbell-Lendrum, D., Holloway, T., & Foley, J. A. (2005). Impact of regional climate change on human health. *Nature, 438*(7066), 310-317.

Perkins, S. E., Pitman, A. J., Holbrook, N. J., & McAneney, J. (2007). Evaluation of the AR4 Climate Models Simulated Daily Maximum Temperature, Minimum Temperature, and Precipitation over Australia Using Probability Density Functions. *Journal of Climate, 20*(17), 4356-4376.

Räisänen, J. (2007). How reliable are climate models? *Tellus A, 59*(1), 2-29. 10.1111/j.1600-0870.2006.00211.x

Ramankutty, N., Foley, J. A., Norman, J., & McSweeney, K. (2002). The global distribution of cultivable lands: current patterns and sensitivity to possible climate change. *Global Ecology and Biogeography, 11*(5), 377-392. 10.1046/j.1466-822x.2002.00294.x

Raper, S. C. B., Gregory, J. M., & Osborn, T. J. (2001). Use of an upwelling-diffusion energy balance climate model to simulate and diagnose A/OGCM results. *Climate Dynamics, 17*(8), 601-613. 10.1007/pl00007931

Root, T. L., Price, J. T., Hall, K. R., Schneider, S. H., Rosenzweig, C., & Pounds, J. A. (2003). Fingerprints of global warming on wild animals and plants. *Nature, 421*(6918), 57-60.

Ruosteenoja, K., Tuomenvirta, H., & Jylhä, K. (2007). GCM-based regional temperature and precipitation change estimates for Europe under four SRES scenarios applying a super-ensemble pattern-scaling method. *Climatic Change, 81*(0), 193-208. 10.1007/s10584-006-9222-3

Sansom, J., & Renwick, J. A. (2007). Climate Change Scenarios for New Zealand Rainfall. *Journal of Applied Meteorology and Climatology, 46*(5), 573-590. doi:10.1175/JAM2491.1

Santer, B. D., Wigley, T. M. L., Schlesinger, M. E., & Mitchell, J. F. B. (1990). *Developing Climate Scenarios from Equilibrium GCM Results, MPI Report Number 47,* Hamburg.

Semenov, & Bengtsson. (2002). Secular trends in daily precipitation characteristics: greenhouse gas simulation with a coupled AOGCM. *Climate Dynamics, 19*(2), 123-140. 10.1007/s00382-001-0218-4

Sorteberg, A., & Kvamstø, N. G. (2006). The effect of internal variability on anthropogenic climate projections. *Tellus A, 58*(5), 565-574. 10.1111/j.1600-0870.2006.00202.x

Sutherst, R. W. (1998). Implications of global change and climate variability for vector-borne diseases: generic approaches to impact assessments. *International Journal for Parasitology, 28*(6), 935-945.

Tebaldi, C., Hayhoe, K., Arblaster, J., & Meehl, G. (2006). Going to the Extremes. *Climatic Change, 79*(3), 185-211. 10.1007/s10584-006-9051-4

Theurillat, J.-P., & Guisan, A. (2001). Potential Impact of Climate Change on Vegetation in the European Alps: A Review. *Climatic Change, 50*(1), 77-109. 10.1023/a:1010632015572

Thuiller, W., Lavorel, S., & Araújo, M. B. (2005). Niche properties and geographical extent as predictors of species sensitivity to climate change. *Global Ecology and Biogeography, 14*(4), 347-357. 10.1111/j.1466-822X.2005.00162.x

Trenberth, K. E. (1999). Conceptual Framework for Changes of Extremes of the Hydrological Cycle with Climate Change. *Climatic Change, 42*(1), 327-339. 10.1023/a:1005488920935

Walpita-Gamage, S. H. P., Hewa, G. A., Subhashini, W. H. C., Daniell, T. M. a., & Kemp, D. (2009). *Modelling the extreme floods of South Australian catchments.* Paper presented at the 18th World IMACS Congress and MODSIM09 International Congress on Modelling and Simulation Cairns, Australia. July 2009.

Whetton, P. H., McInnes, K. L., Jones, R. N., Hennessy, K. J., Suppiah, R., Page, C. M., et al. (2005). *Australian Climate Change Projections for Impact Assessment and Policy Application: A Review.* : CSIRO Marine and Atmospheric Research, Aspendale, Victoria, Australia.

Woodward, F. I. (1987). *Climate and Plant Distribution* Cambridge: Cambridge University Press.

5.   Appendices

Appendix 1: Pattern Scaling Methodology

Pattern scaling is based on the theory that, firstly, a simple climate model can accurately represent the global responses of a GCM, even when the response is non-linear (Raper et al., 2001), and secondly, a wide range of climatic variables represented by a GCM are a linear function of the global annual mean temperature change represented by the same GCM at different spatial and/or temporal scales (Mitchell, 2003; Whetton et al., 2005). Scaling local trends by projections of global warming and comparing these to model projections will allow adaptation needs at the local and regional scale to be assessed. For example, pattern-scaled historical data can be compared with pattern scaling from GCMs.

Pattern scaling involves the following general steps (Lu and Hulme, 2002):

Step 1: Defining the 'master pattern' – a single GCM experiment run (or ideally an ensemble) with a corresponding SRES emissions scenario pattern for one climate variable, such as global mean temperature;

Step 2: Normalising the 'master pattern' - the climate change values for each individual grid cell in the 'master pattern' are normalised by subtracting the 'average' value for the global mean temperature (for that GCM experiment run) from each grid cell. This normalised pattern then represents the degree of warming in each grid cell, per degree global warming;

Step 3: Obtaining scalars – this derives the global warming values per grid cell in a climate pattern, for a time in the future for a given emissions scenario, simulated by a simple climate model such as MAGICC SCENGEN;

Step 4: Scaling the normalised pattern – the pattern of changes for the future time period can be produced by multiplying the normalised pattern in Step 2 by the respective scalar developed in Step 3.

Pattern scaling may be described as follows: for a given climate variable *V*, its anomaly ΔV^* for a particular grid cell (*i*), month (*j*) and year or period (*y*) under an emission forcing scenario SRES A1B:

$$\Delta V_{yij}^* = \Delta T_y \cdot \Delta V_{ij}' \qquad (1)$$

ΔT being the annual global mean temperature change.

The local change pattern value ($\Delta V_{ij}'$) was calculated from the GCM simulation anomaly (ΔV_{yij}) using linear least squares regression, that is, the slope of the fitted linear line.

$$\Delta V_{ij}' = \frac{\sum_{y=1}^{m} \Delta T_y \cdot \Delta V_{yij}}{\sum_{y=1}^{m} (\Delta T_y)^2} \qquad (2)$$

where *m* is the number of future sample periods used, with a 10 year average as a period.

Pattern-scaling does not seem to be a very large source of error in constructing regional climate projections, even for extreme scenarios (Ruosteenoja et al., 2007). However, in applying pattern-scaling, two fundamental sources of error related to its underlying theory need to be addressed: 1) the non-linearity error: the local responses of climate variables, precipitation in particular, may not be inherently linear functions of the global mean temperature change; and 2) noise due to the internal variability of the GCM. Based on the pattern scaling theory, for a given GCM, the linear response change pattern of a climate variable to global mean temperature change represented by the GCM should be obtained from any one of its GHG emission simulation outputs.

Table 9 provides a list of GCMs used in this analysis.

Table 9. GCMs used in SimCLIM precipitation and temperature patterns.

No.	Originating Group(s), Country	Model	SimCLIM name	Horizontal grid spacing(km)
1	Canadian Climate Centre, Canada	CCCMA T47	CCCMA-31	~250
2	Meteo-France, France	CNRM	CNRM-CM3	~175
3	CSIRO, Australia	CSIRO-MK3.0	CSIRO-30	~175
4	Geophysical Fluid Dynamics Lab, USA	GFDL 2.0	GFDLCM20	~200
5	Geophysical Fluid Dynamics Lab, USA	GFDL 2.1	GFDLCM21	~200
6	Centre for Climate Research, Japan	MIROC-H	MIROC-HI	~100
7	Meteorological Institute of the University of Bonn, Meteorological Research Institute of KMA, Germany/Korea	MIUB-ECHO-G	ECHO---G	~400
8	Max Planck Institute for meteorology DKRZ, Germany	MPI-ECHAM5	MPIECH-5	~175
9	Meteorological Research Institute, Japan	MRI	MRI-232A	~250
10	National Center for Atmospheric Research, USA	NCAR-CCSM	CCSM—30	~125
11	Hadley Centre, UK	HADCM3	UKHADCM3	~275
12	Hadley Centre, UK	HADGEM1	UKHADGEM	~125

Appendix 2: SRES Emissions Scenarios (IPCC, 2000)

By 2100 the world will have changed in ways that are difficult to imagine - as difficult as it would have been at the end of the 19th century to imagine the changes of the 100 years since then. Each storyline assumes a distinctly different direction for future developments, such that the four storylines differ in increasingly irreversible ways. Together they describe divergent futures that encompass a significant portion of the underlying uncertainties in the main driving forces. They cover a wide range of key "future" characteristics such as demographic change, economic development, and technological change. For this reason, their plausibility or feasibility should not be

considered solely on the basis of an extrapolation of current economic, technological, and social trends.

- The A1 storyline and scenario family describes a future world of very rapid economic growth, global population that peaks in mid-century and declines thereafter, and the rapid introduction of new and more efficient technologies. Major underlying themes are convergence among regions, capacity building, and increased cultural and social interactions, with a substantial reduction in regional differences in per capita income. The A1 scenario family develops into three groups that describe alternative directions of technological change in the energy system. The three A1 groups are distinguished by their technological emphasis: fossil intensive (A1FI), non-fossil energy sources (A1T), or a balance across all sources (A1B).
- The A2 storyline and scenario family describes a very heterogeneous world. The underlying theme is self-reliance and preservation of local identities. Fertility patterns across regions converge very slowly, which results in continuously increasing global population. Economic development is primarily regionally oriented and per capita economic growth and technological changes are more fragmented and slower than in other storylines.
- The B1 storyline and scenario family describe a convergent world with the same global population that peaks in mid-century and declines thereafter, as in the A1 storyline, but with rapid changes in economic structures toward a service and information economy, with reductions in material intensity, and the introduction of clean and resource-efficient technologies. The emphasis is on global solutions to economic, social, and environmental sustainability, including improved equity, but without additional climate initiatives.
- The B2 storyline and scenario family describes a world in which the emphasis is on local solutions to economic, social, and environmental sustainability. It is a world with continuously increasing global population at a rate lower than A2, intermediate levels of economic development, and less rapid and more diverse technological change than in the B1 and A1 storylines. While the scenario is also oriented toward environmental protection and social equity, it focuses on local and regional levels.

Appendix 3: Methodology for extreme precipitation event analysis based on daily GCM data

This is based on the paper by Li and Ye, (submitted, 2009).

GCM outputs are still the most reliable source of information for future climate scenario projections. With more and more detailed GCM data becoming publicly available, including daily time series, it is now possible to pursue more advanced methods for daily extreme precipitation event analysis, which can be based on the finer temporal results. GCMs have relatively poor performance on simulating precipitation at a regional or local scale compared to the historical observed data. This has seriously limited the direct use of GCM precipitation time series in extreme precipitation event analysis. Dynamic downscaling improves the accuracy at finer scales but only to a limited extent. A major drawback of this method is its high computational demand for only one or two simulation outputs. This makes it very difficult for uncertainty analysis for different emission scenarios and different GCMs. A statistical downscaling technique provides a computationally efficient and hence cost-effective solution that can lead to improved accuracy of GCM results. The results can be used not only in the generation of precipitation time series, but also for the analysis of the possible changes to extreme precipitation events under different climate change scenarios. To date, scientific research has not produced a satisfactory method at a fine spatial scale that readily can be implemented for simulating daily precipitation, particularly for extreme analysis.

Among the wide range of climate variables, precipitation extremes have attracted much research attention because of the potential disasters these may cause to human society and natural systems. Extreme precipitation events are projected to increase with climate change, even in areas where the total precipitation is projected to decrease (Meehl et al., 2007), since global warming will noticeably enhance the hydrological cycle at both global and local scales. In order to adequately assess the climate change impact on extreme precipitation events, the characteristics of GCM-simulated precipitation and its relationship with global warming need to be evaluated (Perkins et al., 2007; Alexandra and Arblaster, 2008). The evaluation of observed and modeled trends has shown that the confidence in GCM projected extremes of precipitation is much less than that of temperature (e.g. Kharin et al., 2007; Kiktev et al., 2007). In general, the magnitude of changes in precipitation extremes simulated by GCMs was found to have a linear relationship with the strength of GHG emissions or in proportion with the global warming trend (Alexander and Arblaster, 2009, Tebaldi et al., 2006), which is in alignment with the linear response theory of pattern scaling.

On the other hand, given the current state of scientific understanding and the limitations of GCMs in simulating the complex climate system, a large ensemble of GCM simulations is more appropriate in climate change projections than using individual GCM simulation outputs, particularly if such projections will be used for impact assessments, because only large ensembles of GCM simulations, sampling the widest possible range of modelling uncertainties, can provide a reliable specification of the spread of possible regional changes (Murphy et al., 2004; Sorteberg and Kvamstø, 2006; Murphy et al., 2007; Räisänen, 2007).

Simulations of extreme precipitation in GCMs cannot be expected to accurately reproduce observed absolute quantities or rates of change. The relatively coarse resolution of GCMs prevents the simulation of phenomena that manifest their intensity mainly at synoptic (i.e., regional) scales (Dai, 2006; Tebaldi et al., 2006). GCM-simulated extreme precipitation intensities are systemically much lower than the observed data (Dai, 2006; Kharin et al., 2007).

In lieu of the above, we present the following method for analyzing the climate change impact on extreme precipitation using daily GCM outputs at their original spatial resolution (i.e. not downscaled) (Li and Ye, 2009). The steps of this method are listed below:
1. Build a General Extreme Value (GEV) distribution for one GCM baseline period (1981-2000 or 1980-1999) for daily data and calculate its extreme precipitation intensity values for 11 selected return periods (5 ,10, 20,30,50,100,150,200,300 year periods);
2. Build GEV distribution for the above GCM based on its future daily data. There are two 20-year period 2046-2055 and 2081-2100 for 3 SRES scenarios A2, A1B and B1 available from the IPCC AR4 data archive.
3. Calculate the extreme precipitation intensity values for the 11 selected return periods as baseline period;
4. Calculate the difference in percentage of the extreme precipitation intensity values between baseline and each future period;
5. Calculate the annual global average mean temperature change between the future periods and the baseline for the above GCM;
6. Normalise the extreme precipitation changes by the linear least square regression method using the following equation:

$$\Delta V_{ij}^{'} = \frac{\sum_{y=1}^{m} \Delta T_y \cdot \Delta V_{yij}}{\sum_{y=1}^{m} (\Delta T_y)^2}$$

where $\Delta V_{ij}'$ is the normalised change value for the grid cell(i) and return period (j); ΔV_{yij} is the change percentage for ΔT_y for global mean temperature change for the future period y; m =6, the number of future sample periods used.

With the use of bi-linear interpolation, a finer-scale change pattern of extreme precipitation is obtained at the required spatial resolution (example in Figure 25).
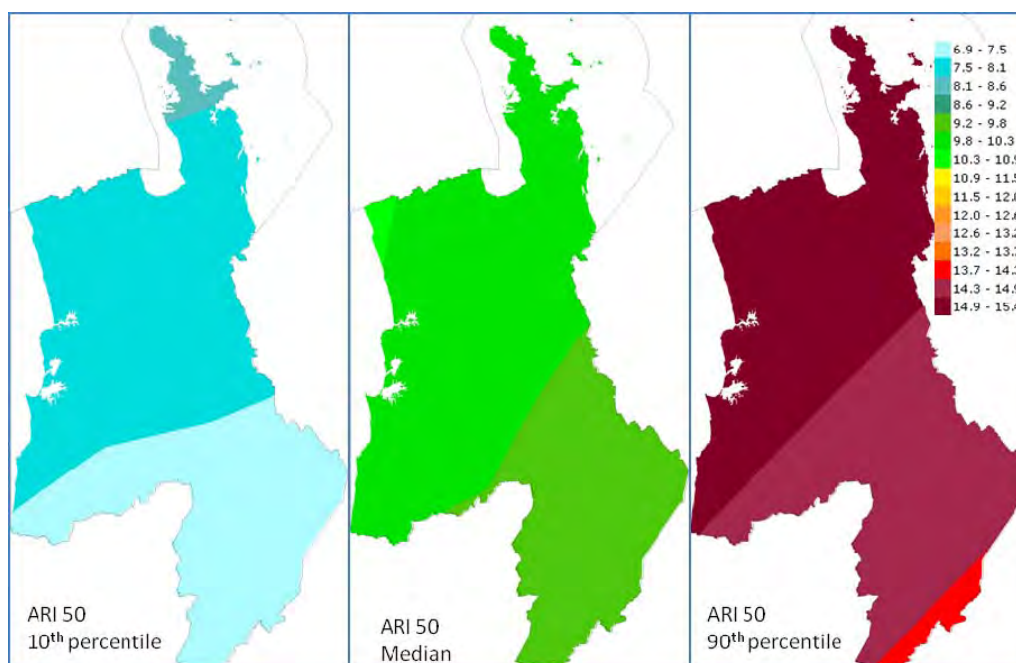

Figure 25. Sample of extreme precipitation change patterns (%) for ARI = 50 years. From left to right, panels show the 10th, Median, and 90th percentile values of 12 GCMs.

By applying the change pattern generated from daily GCM data, it is possible to undertake an extreme precipitation event analysis for the Waikato region.

7. Build GEV distribution from historical gridded daily data of the Waikato region and calculate the extreme precipitation values for the selected return period (10, 20, 50, 100, and 200 years) ;
8. Extract the change pattern values from global change patterns generated in step 6 above;
9. Obtain the global average mean temperature change for the selected study time slices (2020, 2050, and 2100) and GHG emission scenarios (A1FI, A1B and B1) in mid climate sensitivity using the SimCLIM software.
10. Calculate the extreme precipitation values by manipulating the change patterns with global mean temperature using the following equation:

$$P_1 = P_0 \cdot (1 + \Delta P / 100 \times \Delta GMT_1)$$

Where, P_1 and P_0 are the future and baseline extreme precipitations, respectively; ΔP is the change percentage generated from GCM data; and ΔGMT (the scalar) is the change of global mean temperature increase in a future time slice.

In summary, this method can be viewed as an extension of the pattern scaling method to extreme event analysis. Preliminary work using the method for New Zealand and Australia extreme rainfall analysis has generated improved results that conform to other scientific research findings.

Limitations and future development

No statistical downscaling method was involved in this method. Daily GCM precipitation outputs were analyzed in their original spatial resolution in order to retain the extreme precipitation change trend of GCMs. A statistical downscaling method is under development by Climsystems Ltd, which is expected to reflect the extreme precipitation change trend of GCMs in higher spatial resolution with more local information.

MfE (2008) provided a table for extreme precipitation change against global warming. This table recommends that *percentage* adjustments are applied to extreme rainfall per 1 degree Celsius of warming, for a range of ARIs or return periods for the duration of 10 minutes to 72 hours. The entries for the 10-minute duration are based on the theoretical increase in the amount of water held in the atmosphere for a 1 degree increase in temperature (8%). Entries for other durations are based on logarithmic (in time) interpolation between the 10-minute and 24-hour rates.

Table 10 provides the list of GCMs used for this analysis.

Table 10. GCMs used in SimCLIM extreme precipitation analysis.

No.	Originating Group(s), Country	Model	SimCLIM name	Horizontal grid spacing(km)
1	Bjerknes Centre for Climate Research, Norway	BCCR	BCCRBCM2	~175
2	Canadian Climate Centre, Canada	CCCMA T47	CCCMA-31	~250
3	Meteo-France, France	CNRM	CNRM-CM3	~175
4	CSIRO, Australia	CSIRO-MK3.5	CSIRO-35	~175
5	Geophysical Fluid Dynamics Lab, USA	GFDL 2.0	GFDLCM20	~200
6	Geophysical Fluid Dynamics Lab, USA	GFDL 2.1	GFDLCM21	~200
7	Institute Pierre Simon Laplace, France	IPSL	IPSL-CM40	~275
8	Centre for Climate Research, Japan	MIROC-M	MIROCMED	~250
9	Meteorological Institute of the University of Bonn, Meteorological Research Institute of KMA, Germany/Korea	MIUB-ECHO-G	ECHO---G	~400
10	Max Planck Institute for meteorology DKRZ, Germany	MPI-ECHAM5	MPIECH-5	~175
11	Meteorological Research Institute, Japan	MRI	MRI-232A	~250
12	National Center for Atmospheric Research, USA	NCAR-CCSM	CCSM—30	~125

Appendix 4: Computation of the Potential Evapotranspiration Deficit, PED

The water balance calculation used to derive the Potential Evapotranspiration Deficit (*PED*) index assumes that the water gains and losses to the soil profile are typically in balance (Mullan et al., 2005). Provided that water is non-limiting, the balance for a given rainfall period can be written as:

P = PET + Ro + D ± ΔS

Where *P* is precipitation, *PET* is potential (or upper limit) evapotranspiration, *Ro* is surface runoff, *D* is drainage loss through percolation, and *ΔS* is the change in water storage. For the purposes of this study, *PET* is calibrated for pasture water use.

In principle, for each day,

$S = S_{d-1} + P - PET - Ro - D$
Where *S* is the new storage, and S_{d-1} is the water storage for the previous day.

Field capacity water storage is defined by the Available Water Capacity *(AWC)*, which was taken to be 150 mm for this study (Mullan et al., 2005). Rainfall in excess of field capacity is assumed to be lost to the water balance by runoff and drainage.

if $S_{d-1} + P - PET > AWC$
then $(S_{d-1} + P - PET) - AWC = (Ro + D)$

As *S* is reduced, it becomes increasingly difficult for plants to extract water from the soil, and water transpiration decreases. Here we have used a method for estimating constrained water use by assuming evapotranspiration (ET) continues at its potential rate until half *AWC* is depleted, following which it ceases until further rain occurs.

if $S < ½(AWC)$
then $ET = 0$

The difference between the subsequent soil water-restricted evapotranspiration, *(RET),* and the atmospheric potential evapotranspiration for the period *(PET)*, is referred to here as the potential evapotranspiration deficit *(PED)* and is incremented on a daily basis.

$PED = PED_{d-1} + (PET - RET)$
In effect, *PED* is approximately equivalent to the amount of water that would need to be added by rainfall or irrigation to keep pasture growing at its daily potential rate.

PED was accumulated daily for the July to June year, beginning from zero each year. Note that the soil moisture deficit carries over from one year to the next, even though *PED* is reset at the beginning of each July-June period. The water balance calculation was initiated on 1 January 1972, so there was a potentially non-zero starting value of soil moisture deficit at the beginning of July 1972.

Appendix 5: Calculation of the Temperature Humidity Index (THI)

The Temperature Humidity Index (THI) was calculated using the following equation (Mayer et al., 1999):

$$THI = T + 0.36T_d + 41.2$$

Where, *T* is air temperature (degrees Celsius) and T_d is the dew point temperature (°C) which was calculated as follows:

$$T_d = \frac{b\gamma(T,RH)}{a - \gamma(T,RH)}$$

Where

$$\gamma(T,RH) = \frac{aT}{b+T} + \ln(RH/100)$$

Where the temperatures are in degrees Celsius (°C) and, *ln* refers to the natural logarithm, RH refers to relative humidity.

The constants are:
a = 17.271, *b* = 237.7 °C

The hourly temperature *T* was calculated from the daily maximum and minimum temperature using the method by De Wit et al., 1978. Temperature data were divided into two sets: from sunrise to 1400h and from 1400 to sunrise hour. The method assumes *Tmax* at 1400 and *Tmin* at sunrise. Therefore, the temperature for hour *h* was calculated using the following equations:

$$T(h) = TAVE - AMP(\cos(\pi(h - RISE)/(14 - RISE))), \text{ if h>RISE and h<=14}$$
$$T(h) = TAVE + AMP(\cos(\pi(h - 14)/(RISE - 14))) \text{ , for other hours}$$

Where, *h* is the local hour of a day (0100-2400), RISE is the sunrise hour, TAVE and AMP are defined as:
TAVE= (TMAX+TMIN)/2.0, AMP = (TMAX-TMIN)/2.0

The average temperature of the hottest 3 hours in each day was used for the THI calculation.

Appendix 6: Methodology for generating sea level rise patterns

Global-mean sea-level rise scenarios are readily available and are regularly updated by the IPCC. To date, most coastal impact and adaptation assessments have ignored regional variations in sea-level scenarios, largely due to a lack of technical guidance and access to the necessary data in a usable form. Nevertheless, regional and local assessments would benefit from considering the components of sea-level change on a more individual basis, since the uncertainty for sea-level change during the 21st century at any site is very likely to be larger than the global-mean scenarios suggest.

Meteo-oceanographic factors
Regional variations in atmospheric circulation, ocean circulation and warming rates, spatial variations in mass redistribution and the interactions between them can lead to significant deviations of regional sea-level change from the globally-averaged trend. There are two main methods for estimating regional variations using modelled data.

Pattern scaling

The regional pattern of thermal expansion under SRES forcing can be approximated using a pattern-scaling method similar to that previously applied for other climate variables (e.g. Santer *et al.*, 1990; Carter *et al.*, 2001). In applying the pattern-scaling method to sea level, "standardised" (or "normalised") patterns of regional thermal expansion change, as produced by coupled AOGCMs, are derived by dividing the average spatial pattern of change for a future period (e.g. 2071-2100) by the corresponding global-mean value of thermal expansion for the same period. The resulting standardised sea-level pattern is thereby expressed per unit of global-mean thermal expansion. The pattern-scaling approach has been formalised within an integrated assessment modelling system called SimCLIM.

Vertical land movements (uplift and subsidence)

In general, during the 21st century, vertical land movement is expected to be less than the rise resulting from oceanographic changes in most locations; indeed, in areas undergoing land uplift, this process may help counteract some of the effects of a rise in global mean sea level. However, while some modelling may be available, determining local and regional variations in vertical land movements can be problematic as long data sets are required.

The observed sea level records have been used to project future sea-level rise, using a simple extrapolation of the observed relative sea-level change trend into the future. This is theoretically debatable as it fails to differentiate sea level rise caused by historical climate change, from changes attributable to local land movements. By superimposing the extrapolation of observed sea-level change trends onto the projections of global warming related sea-level rise (e.g. those from climate models), such a procedure would lead to "double-counting" of any sea-level rise resulting from large-scale processes associated with global warming. Therefore, to estimate the contribution of local land movement to relative sea-level change in the future, the climate change related portion of sea-level rise needs to be subtracted from the observed local trend.

We employed the following equation to calculate the normalised sea surface elevation patterns, (or sea surface height above the geoid, ZOS), termed *DZOS (unit: cm/cm ΔGSLR)*:

$$DZOS_{ij} = \left\{ \left(ZOS_{ij2090} - ZOS_{ij1990} \right) + \Delta GSLR \right\} / \Delta GSLR$$

Where,
$\Delta GSLR$ is the global mean annual sea level change due to thermal expansion

$$\Delta GSLR = ZOSTOGA_{2090} - ZOSTOGA_{1990}$$

Where,
ZOSTOGA is the global mean thermosteric sea level change
i, j denote the latitude and longitude position;
2090 is the average of 2080-2100; 1990 is the average of 1980-2000.

The data source of 1x1 degree global latitude longitude $\left(ZOS_{ij2090} - ZOS_{ij1990} \right)$ and the global annual mean sea level rise (*ΔGSLR*) due to thermal expansion were processed by Jonathan Gregory for IPCC (ref: http://ncas-climate.nerc.ac.uk/~jonathan/data/ar4_sealevel/). Thirteen GCM (SRES A1B) runs, which have both local *ZOS* and *ZOSTOGA* data, were used in SimCLIM (see Table III). Projected global average sea level rise values during the 21st century and its components under SRES marker scenarios were taken from IPCC AR4 chapter 10, Table 10.7. A cubic equation was used for fitting the curves of the transient changes.

Table 11 provides the list of GCMs used for this analysis.

Table 11. GCMs used in SimCLIM sea level change patterns.

No.	Originating Group(s), Country	Model	SimCLIM name	Original spatial resolution
1	Canadian Climate Centre, Canada	CCCMA T47	CCCMA-31	96*192
2	CSIRO, Australia	CSIRO-MK3.0	CSIRO-30	~175
3	Geophysical Fluid Dynamics Lab, USA	GFDL 2.1	GFDLCM21	200*360
4	NASA/Goddard Institute for Space Studies, USA	GISS-E-H	GISS—EH	180*360
5	NASA/Goddard Institute for Space Studies, USA	GISS-E-R	GISS—ER	46*72
6	NASA/Goddard Institute for Space Studies, USA	GISS-AOM	GISS_AOM	60*90
7	Centre for Climate Research, Japan	MIROC-H	MIROC-HI	320*320
8	Centre for Climate Research, Japan	MIROC-M	MIROCMED	192*256
9	Meteorological Institute of the University of Bonn, Meteorological Research Institute of KMA, Germany/Korea	MIUB-ECHO-G	ECHO---G	117*128
10	Max Planck Institute for meteorology DKRZ, Germany	MPI-ECHAM5	MPIECH-5	180*360
11	Meteorological Research Institute, Japan	MRI	MRI-232A	111*144
12	National Center for Atmospheric Research, USA	NCAR-CCSM	CCSM—30	395*320
13	Hadley Centre, UK	HADCM3	UKHADCM3	144*288